



## Diploma Thesis

# The Effect of SO<sub>2</sub> on the Absorption of CO<sub>2</sub> using Potassium Carbonate Solution

provided for

**Cooperative Research Centre for Greenhouse Gas  
Technologies (CO2CRC)**

**Vorgelegt von:**

David Wappel Bakk. techn.  
0135050

**Betreuer/Gutachter:**

Dr. Sjoerd van Zijll de Jong  
Ao.Univ.-Prof. Dipl.-Ing.Dr.techn. Josef Draxler

Leoben, 05.03.2007

## **EIDESSTATTLICHE ERKLÄRUNG**

Ich erkläre an Eides statt, dass ich die vorliegende Diplomarbeit selbständig und ohne fremde Hilfe verfasst, andere als die angegebenen Quellen und Hilfsmittel nicht benutzt und die den benutzten Quellen wörtlich und inhaltlich entnommenen Stellen als solche erkenntlich gemacht habe.

## **DANKSAGUNG / ACKNOWLEDGMENT**

Für die Möglichkeit meine Diplomarbeit in Australien an der University of Melbourne zu schreiben, sowie für die gute Betreuung in Österreich möchte ich mich recht herzlich bei Herrn Prof. Dr. Josef Draxler bedanken. Ohne Herrn Prof. Draxler wäre es nicht möglich gewesen, diese einzigartige Chance zu nützen und dadurch meine fachlichen aber vor allem persönlichen und kulturellen Erfahrungen zu verbessern.

I would especially like to acknowledge both my advisor Dr Sjoerd van Zijl de Jong and colleague Michael Simioni for their help and support preparing this thesis during my time in Melbourne. Both always had time for any problems, questions and comments with my work and gave significant guidance to me that has ensured the completion of my thesis. Without their support it is difficult to see how my research could have been completed so successfully. Also, their friendship was an important part that made my experience in Melbourne so enjoyable and worthwhile.

Furthermore, I would like to express my gratitude to Professor Geoff Stevens and Dr Sandra Kentish for giving me the opportunity to complete my thesis at The University of Melbourne, giving me support and access to all the necessary laboratories, equipment and consumables that has enable my research work to be completed so successfully. The meetings, their technical discussions, helpful advice and scientific knowledge were essential to the completion and success of this work.

Der größte Dank gilt aber meinen Eltern und meiner Familie, die mich zur jeder Zeit unterstützt haben und ohne die es sicherlich nicht möglich gewesen wäre, mein Studium so erfolgreich durchzuführen. Auch die Möglichkeit eines Auslandsemesters und das Schreiben der Diplomarbeit in Australien, waren unvergesslich schöne, wichtige und sehr lehrreiche Zeiten, die ohne die Unterstützung meiner Eltern niemals mögliche gewesen wären.

Großen Dank auch an alle Freunde, die mich während meiner Studienzzeit unterstützt haben und mit denen ich gemeinsam diverse studentische Abendaktivitäten unternommen habe.

## Kurzfassung

### Der Einfluss von SO<sub>2</sub> auf die Absorption von CO<sub>2</sub> in Kaliumcarbonat

Die meisten anerkannten Forscher sind sich heutzutage einig, dass die weltweite Reduktion von CO<sub>2</sub> Emissionen und die damit verbundene Verringerung des Treibhauseffektes nur durch weit reichendes Abtrennen und Sequestrieren von CO<sub>2</sub> möglich ist. Das Abtrennen, in den meisten Fällen Absorbieren, von CO<sub>2</sub> ist der mit Abstand teuerste Prozessschritt und viel Forschung wird weltweit unternommen, um eine Optimierung dieses Prozesses zu erreichen. Die gleichzeitige Absorption von mehreren Schadstoffen, wie CO<sub>2</sub>, SO<sub>2</sub> und NO<sub>x</sub> aus Rauchgasen in eine Kaliumcarbonatlösung (K<sub>2</sub>CO<sub>3</sub>) könnte eine mögliche Kostenoptimierung darstellen. Diese Arbeit im Speziellen, beschäftigt sich mit dem Einfluss von SO<sub>2</sub> auf die Gleichgewichtskurve und das Absorptionsvermögen von CO<sub>2</sub> in eine 30%ige Kaliumcarbonatlösung.

Durch die Absorption von SO<sub>2</sub> in Kaliumcarbonat kommt es zu einer Änderung der Gleichgewichtskurve zwischen CO<sub>2</sub> und K<sub>2</sub>CO<sub>3</sub>. Diese Änderung hat natürlich Einfluss auf das Absorptionsvermögen und den Wirkungsgrad der CO<sub>2</sub> Absorptionsanlage. Es ist wichtig herauszufinden, wie sich die Gleichgewichtskurve von CO<sub>2</sub> durch das Absorbieren von SO<sub>2</sub> ändert und wie diese Änderung den Wirkungsgrad des Prozesses oder der Anlage beeinflusst. Der Zusammenhang zwischen der Menge an absorbiertem SO<sub>2</sub> und der Änderung der Gleichgewichtskurve oder des Partialdruckes, zeigt diese Auswirkungen direkt an.

Weiters ist eine Identifikation der ablaufenden Reaktion und der entstehenden Verbindungen durch die Absorption von SO<sub>2</sub> wichtig. Die Flüchtigkeit und die Löslichkeit des gebundenen Schwefels in der Kaliumcarbonatlösung zeigen Möglichkeiten auf, wie das gelöste SO<sub>2</sub> aus der Lösung wieder entfernt werden kann um einen kontinuierlichen Absorptions / Stripping Kreislauf zu gewährleisten.

## Abstract

### The Effect of SO<sub>2</sub> on the Absorption of CO<sub>2</sub> using Potassium Carbonate

Today, most scientists are confident that carbon dioxide mitigation by carbon capture and storage is the most feasible option to significantly reduce the level of carbon dioxide emissions and with that slow climate change and even reduce the impact of the greenhouse effect. The capture of CO<sub>2</sub>, which in most approaches is by absorption, is at present the most cost intensive stage and hence significant scientific effort has been directed to find more effective technologies. The simultaneously multi-component absorption of CO<sub>2</sub>, SO<sub>2</sub> and NO<sub>x</sub> from flue gas using potassium carbonate (K<sub>2</sub>CO<sub>3</sub>) solution is believed to be both a more cost effective and attractive technology. Based on such a capture process, it was the aim of this work to investigate the effect of SO<sub>2</sub> on the vapour–liquid equilibrium (VLE) curve and absorption efficiency of carbon dioxide using a 30w% unpromoted potassium carbonate solution.

As consequence of the absorption of SO<sub>2</sub> into the potassium carbonate solution, it would be expected that the VLE curve of the CO<sub>2</sub>-K<sub>2</sub>CO<sub>3</sub> system would change. This change in the VLE curve implies an inherent effect on the absorption performance and efficiency of the CO<sub>2</sub> capture unit operation. For the purposes of process design and operation it is important to know how the CO<sub>2</sub> equilibrium curve will change with the absorption of SO<sub>2</sub> and how this affects the CO<sub>2</sub> capture performance and efficiency. In this thesis, a direct relationship between the absorbed SO<sub>2</sub> and the change in the CO<sub>2</sub> equilibrium partial pressure for the carbonate system was shown both qualitatively and quantitatively.

Furthermore, identification of the underlying reactions and the species formed during the absorption of SO<sub>2</sub> by the carbonate solution was another aspect investigated in this thesis. Quantification of the resulting sulphur species was used to investigate their volatility and solubility in the carbonate solution and used to investigate possible methods to regulate the concentration of absorbed SO<sub>2</sub>.

## Index of Contents

<b>1</b>	<b>INTRODUCTION.....</b>	<b>4</b>
1.1	General Introduction .....	4
1.1.1	Global Warming and the Greenhouse Effect.....	4
1.1.2	Carbon Capture and Storage (CCS) .....	8
1.1.2.1	Different Capture Technologies.....	9
1.1.2.2	Transport and Storage of CO <sub>2</sub> .....	10
1.1.2.3	Costs of CCS.....	10
1.2	Purpose of the Study .....	11
1.3	Goals of this Study.....	13
<b>2</b>	<b>THEORETICAL PART.....</b>	<b>14</b>
2.1	Basics about Gas Absorption.....	14
2.1.1	Physical Absorption.....	14
2.1.1.1	Vapour Liquid Equilibrium.....	14
2.1.1.2	Two Film Theory.....	18
2.1.2	Chemical Absorption .....	22
2.1.2.1	Chemical Absorption of CO <sub>2</sub> in Alkaline Solutions.....	22
2.1.2.2	Chemical Absorption of Sulphur Dioxide in Alkaline Solutions.....	26
2.2	The Gas Absorption Process .....	26
2.2.1	Equipment and Design Parameters.....	26
2.2.2	Flow Sheet and Mode of Operation.....	28
2.2.3	Absorption and Stripping Diagrams.....	29
2.3	Alkali – Metals (Potassium Carbonate) as an Absorption Medium .....	32
2.3.1	CO <sub>2</sub> Absorption with Potassium Carbonate.....	32
2.3.1.1	Properties of the Aqueous Potassium Carbonate Solution .....	32
2.3.1.2	Hot Potassium Carbonate (Benfield) Process .....	33
2.3.2	SO <sub>2</sub> Absorption with Alkali – Metals .....	34
2.3.2.1	Double Alkali Process.....	34
<b>3</b>	<b>EXPERIMENTAL PART .....</b>	<b>36</b>
3.1	The Equilibrium Rig.....	36
3.1.1	Design and Schematic.....	36



3.1.2	Operation Mode.....	37
3.1.3	Loading of the Solutions.....	38
3.2	Analysis of Carbonate.....	39
3.2.1	Titration.....	39
3.2.1.1	Calculation of Carbonate and Bicarbonate Concentration .....	39
3.2.1.2	Diagram of a $K_2CO_3$ Titration.....	41
3.2.2	Gas Chromatography .....	41
3.2.2.1	The Calibration Curve.....	43
3.3	Analyses of Sulphur in Liquid Solutions .....	43
3.3.1	Analysis with FTIR (Fourier Transform Infrared Spectroscopy) .....	44
3.3.1.1	Basics about Infrared (IR) and FTIR Spectroscopy.....	44
3.3.1.2	Samples Preparation and Background.....	44
3.3.2	Analysis with ICP - AES (Inductively Coupled Plasma - Atomic Emission Spectrometer).....	45
3.3.2.1	Basic about Atomic Spectroscopy .....	45
3.3.2.2	Basics about ICP - AES.....	45
3.3.2.3	Sample and Standard Preparation .....	46
<b>4</b>	<b>RESULTS / DISCUSSION .....</b>	<b>47</b>
4.1	The $CO_2$ Equilibrium Curve.....	47
4.1.1	Calculation of the $CO_2$ Equilibrium Partial Pressure from the Experimental Results.....	47
4.1.2	Equilibrium Curves for the System $CO_2 - K_2CO_3$ .....	50
4.2	Solvent Concentration of Sulphur .....	52
4.3	Sulphur Speciation.....	53
4.3.1	Qualitative Analysis of the Formed Species.....	53
4.3.2	Determination of the Sulphite ( $SO_3^{2-}$ ) Concentration .....	55
4.4	The Effect of $SO_2$ on the Equilibrium Curve of $CO_2$ .....	56
4.4.1	Equilibrium Curves for the System $SO_2 - CO_2 - K_2CO_3$ .....	56
4.4.2	The Effect of Solvent Sulphur Concentration on the $CO_2$ Equilibrium Partial Pressure .....	61
4.5	Properties, Effects and Solutions for the Absorbed $SO_2$ .....	62
4.5.1	Volatility of Absorbed $SO_2$ .....	62
4.5.2	Solubility of Substances in Solution.....	63
4.5.3	Approximate Concentrations of Dissolved $SO_2$ .....	64



---

<b>5</b>	<b>SUMMARY</b> .....	<b>66</b>
<b>6</b>	<b>INDEXES</b> .....	<b>70</b>
6.1	References .....	70
6.2	Tables .....	73
6.3	Graphics .....	74

# 1 Introduction

## 1.1 General Introduction

### 1.1.1 Global Warming and the Greenhouse Effect

“An overwhelming body of scientific evidence indicates that the Earth’s climate is rapidly changing, predominantly as a result of increase in greenhouse gases caused by human activities.” [14, Part I, pp. 3]

“The causal link between greenhouse gases concentration and global temperatures is well established, founded on principles established by scientists in the nineteenth century.” [14, Part I, pp. 7]

Today, few scientists deny that combustion of fossil fuels is one of the major causes of global warming and the greenhouse effect. Figure 1 illustrates the greenhouse effect and shows the problems that occur with the increase of CO<sub>2</sub> and other greenhouse gases. By increasing the concentration of greenhouse gases, more of the infrared radiation and with that energy will be absorbed and retained within the atmosphere which leads to an unavoidable increase of temperature in the lower atmosphere.

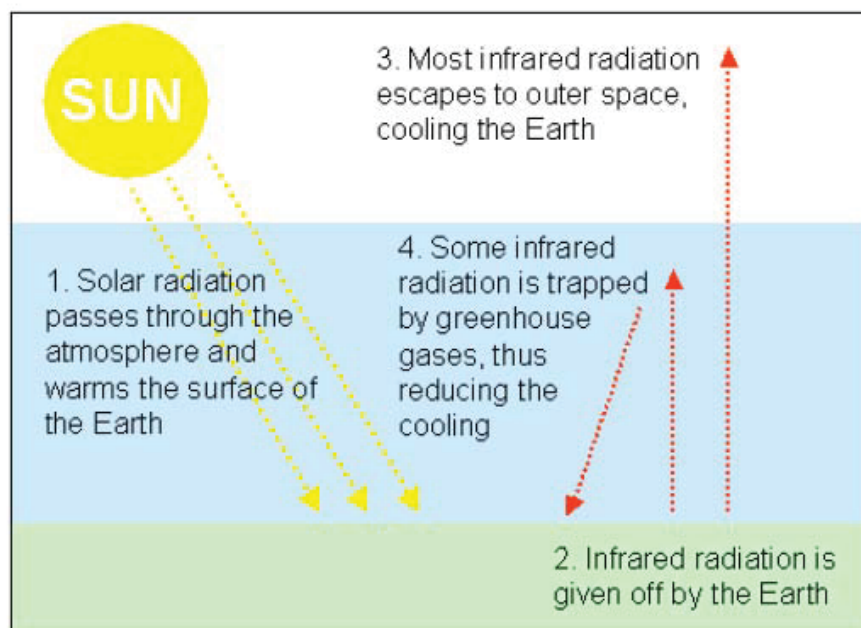


Figure 1: The greenhouse effect [14].

Since the pre – industrial times (around 1750), the concentration of carbon dioxide in the atmosphere has increased from 280ppm to 380ppm [14]. Including other greenhouse (Kyoto) gases which with CO<sub>2</sub> are responsible for global warming, particularly methane and nitrous

oxide, the CO<sub>2</sub> equivalent concentration (CO<sub>2</sub>e) in the atmosphere is now around 430ppm and rising at about 2.3 ppm per year [14].

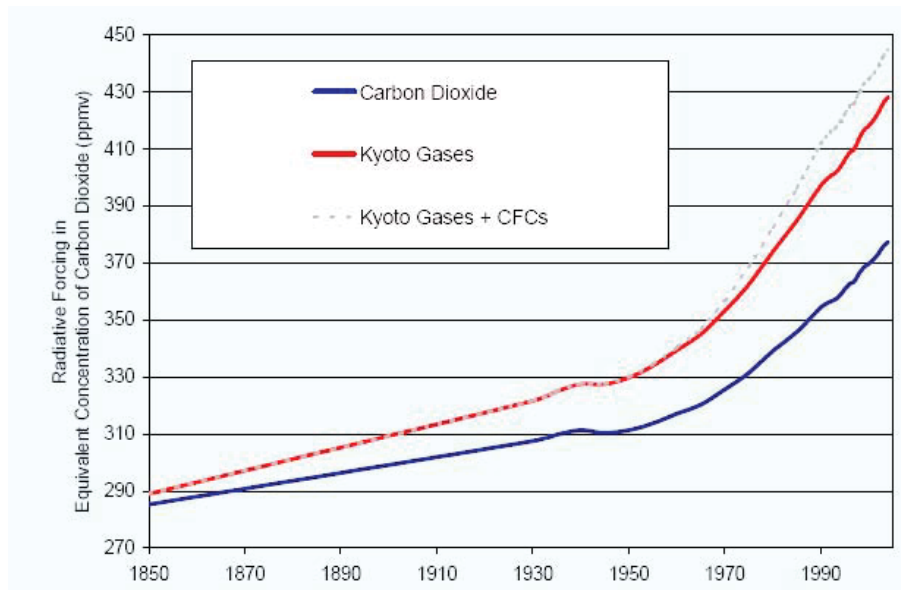


Figure 2: Atmospheric CO<sub>2</sub> concentration from 1850 – 2000 [14].

Shown in Figure 2 is the increase of CO<sub>2</sub> and greenhouse (Kyoto) gases starting from 1850 until today. For future trends and scenarios, various models were used that predict a prognosis within a wide range and with high uncertainty, but in all cases the concentration of the greenhouse gases increase significantly. Figure 3 shows some possible trends and the IPCC Report for Climate Change [15] and the IPCC Special Report -Emissions Scenarios [16] provide more detailed information and explanations for the different scenarios.

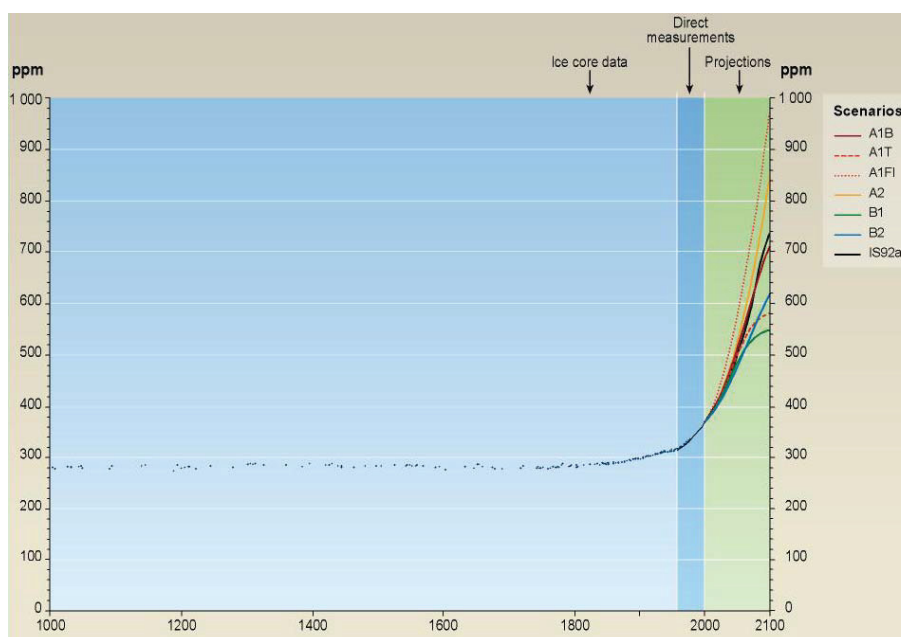


Figure 3: Past and future CO<sub>2</sub> atmospheric concentrations [15].

As a consequence of the greenhouse effect, the temperature is observed to increase with rising of the CO<sub>2</sub> concentration in the atmosphere. Our earth has warmed by 0.7°C since 1900 [14] and with continued burning of more fossil fuels the warming will increase significantly. Based on the different models Figure 4 illustrates the possible temperature change for the next 100 years.

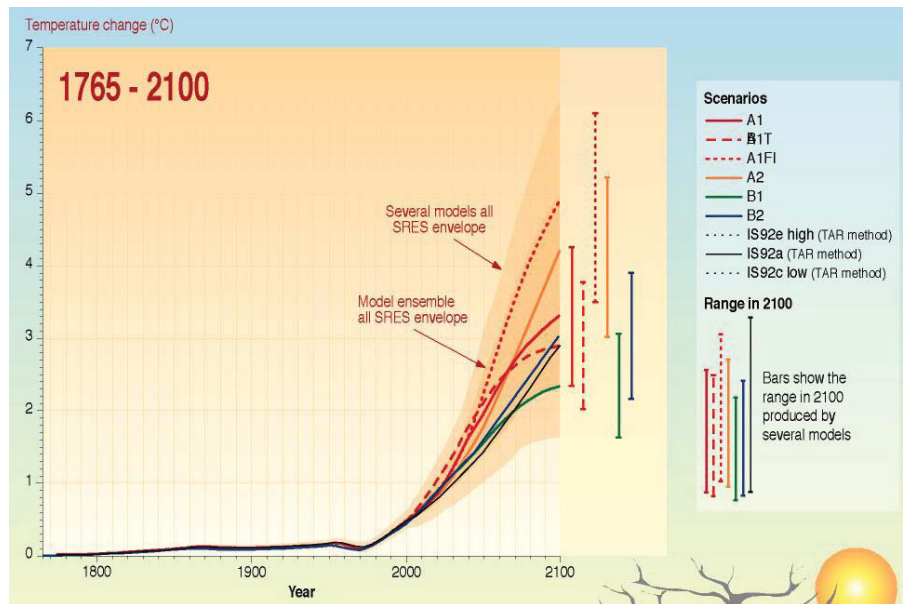


Figure 4: Variations of the Earth's surface temperature from 1765 to 2100.

As seen in Figure 3 and Figure 4 there is a direct link between the atmospheric CO<sub>2</sub> concentration and the rising of the temperature. This climate change will have an effect on health, environment, food production and access to water for people all over the world.

“Most climate models show that a doubling of pre-industrial levels of greenhouse gases is very likely to commit the Earth to a rise of between 2 – 5°C in global mean temperatures. This level of greenhouse gases will probably be reached between 2030 and 2060.” [14, Part I, pp.2]

The economic effects of climate change are significant. Stern [14] predicts that the overall costs of climate change will be equivalent to losing at least 5% of global GDP (Gross Domestic Product) each year, now and forever if we do not act. The only way to reduce the impact of global warming is to stabilize the concentration of greenhouse gases in the atmosphere at the lowest possible level. The costs for stabilizing the concentration at 500 – 550ppm CO<sub>2</sub>e to reducing the greenhouse effect and avoid the worst impact, would only be about 1% of the global GDP each year if we start strong actions now [14]. Even if Stern's pessimistic conclusions are overestimated and the effects are not so significant, it is clear that actions against global warming have to be undertaken soon.

The main actions against the greenhouse effect are:

- Conservation and energy efficiency
- Renewable energy
- Nuclear energy
- Coal to gas substitution
- Carbon Capture and Storage (CCS)

From an environmental and sustainability point of view, nuclear energy cannot be seen as a satisfying solution against global warming. Even if energy efficiency, renewable energy sources and coal to gas substitution will be commonly applied, the ambitious goal of a stable CO<sub>2</sub> concentration in the area of 500 – 600ppm is unlikely to be achieved. To date, Carbon Capture and Storage (CCS) is the only foreseeable solution for a significant reduction of the carbon dioxide emissions.

“CCS involves the use of technology, first to collect and concentrate the CO<sub>2</sub>, transport it to a suitable storage location, and then store it away from the atmosphere for a long period of time. CCS would thus allow fossil fuels to be used with low emissions of greenhouse gases.” [13, pp. 19]

The data presented in Figure 5 [21] shows that based on the IS92a scenario [22] possible reduction of future atmospheric CO<sub>2</sub> concentration through the application of CCS. The IS92a is a middle range scenario (see Figure 3 and Figure 4) which is most widely accepted and predicts an atmospheric CO<sub>2</sub> concentration of about 700ppm in the year 2100. This scenario also includes very significant increase in renewable energy and energy efficiency, which for on their own are not easily achieved. With the application of intensive CCS to power plants and also to transportation, the atmospheric concentration of CO<sub>2</sub> could be reduced to about 570ppm in the year 2100 [21].

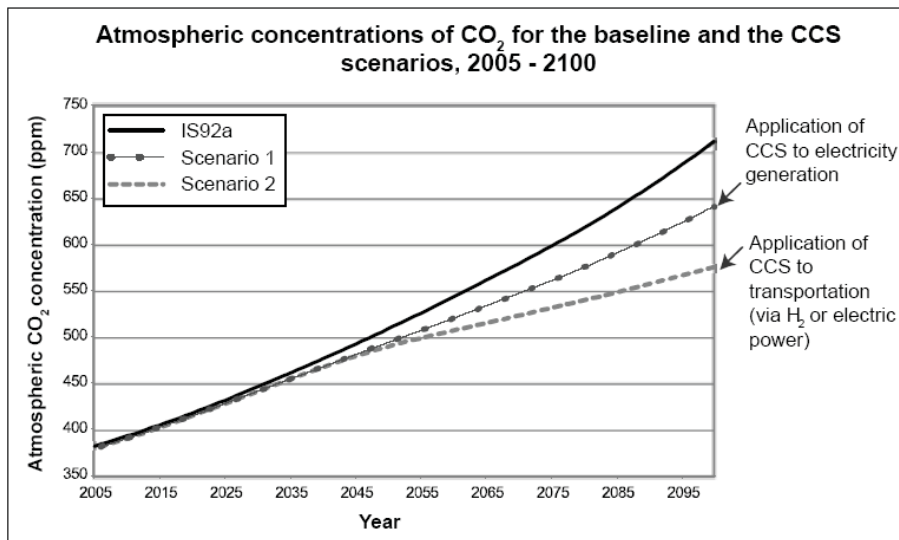


Figure 5: Potential reduction of atmospheric CO<sub>2</sub> concentration with CCS.

### 1.1.2 Carbon Capture and Storage (CCS)

As mentioned earlier, Carbon Capture and Storage consists of three main parts, captures, transport and storage of the CO<sub>2</sub>.

Figure 6 illustrates the possibilities of Carbon Capture and Storage. Electricity or hydrogen is produced by burning of fossil fuels, the CO<sub>2</sub> is captured and then transported to the different sinks, such as geological or ocean storage.

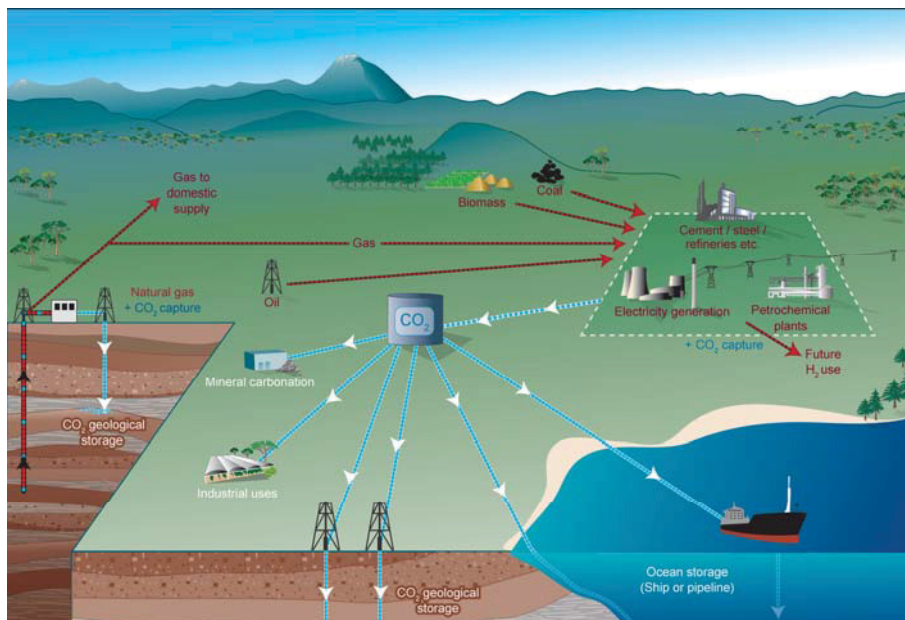


Figure 6: Schematic diagram of possible CCS Systems [17].

### 1.1.2.1 Different Capture Technologies

Apart from natural gas processing, where CO<sub>2</sub> capture is already an applied and proven technology, there are three main approaches for capturing the CO<sub>2</sub> generated from a primary fossil fuel (coal, natural gas or biomass).

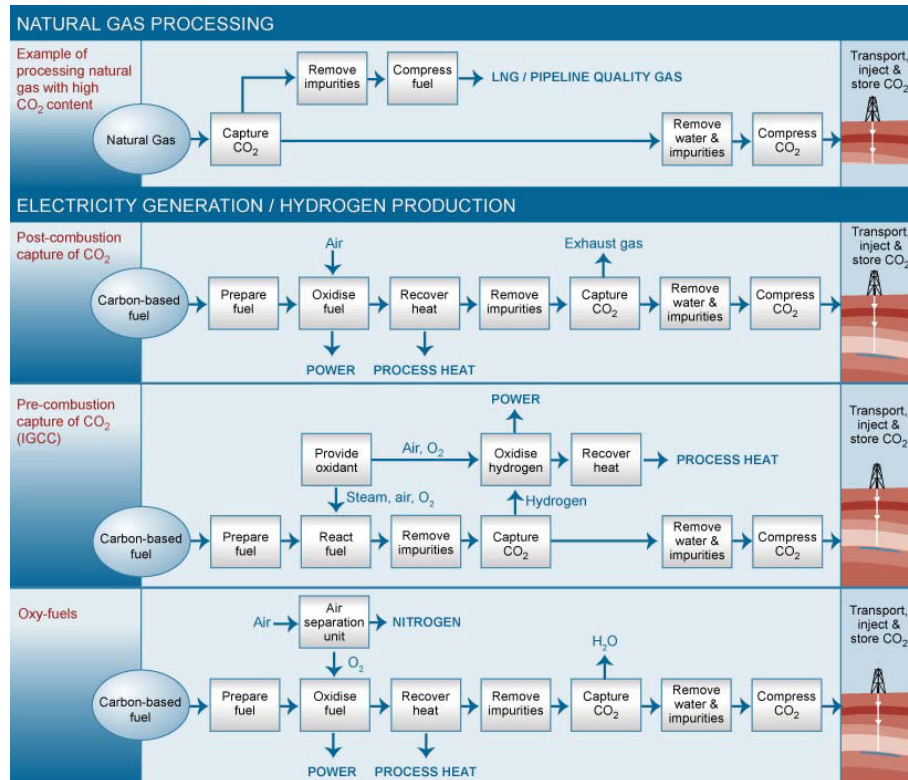


Figure 7: Overview of CO<sub>2</sub> capture processes and systems [17].

- Post-combustion:** Capture of CO<sub>2</sub> from a flue gas produced after the burning of the primary fuel with air. Normally liquid solvents like amines or alkaline – carbonates are used to absorb the CO<sub>2</sub> into the solvent. Typical CO<sub>2</sub> flue gas concentrations are between 3-15%, in which the major component is N<sub>2</sub> from air. Post-combustion can be installed in existing power plants, without major modifications.
- Pre-combustion:** A synthesis gas mixture, mainly containing CO and H<sub>2</sub> is formed by processing the primary fuel with steam and air or oxygen. In a shift reactor additional H<sub>2</sub> is produced and the CO is converted into CO<sub>2</sub>. CO<sub>2</sub> is then captured from the hydrogen. Advantages over the post-combustion are the higher CO<sub>2</sub> concentrations, typically in a range of 15 – 60% and the higher pressures which enhances the capture performance.
- Oxyfuel combustion:** The primary fuel is burned with pure oxygen instead of air, so mainly CO<sub>2</sub> and water vapour are formed. CO<sub>2</sub> then can be captured easily by condensing out the water. The flue gas stream has high CO<sub>2</sub> concentrations up to

80% but a significant amount of energy is necessary to separate the oxygen from air [13].

### 1.1.2.2 Transport and Storage of CO<sub>2</sub>

After capture, the pure gaseous CO<sub>2</sub> is compressed to a pressure above 80 bar and then transported in a pipeline to the storage site. CO<sub>2</sub> can also be liquefied and transported in ships, road or rail tankers.

Storage of CO<sub>2</sub> can be realised either in the ocean or geological formations. In geological formations there are basically three main options, storage in depleted oil and gas reservoirs, use of CO<sub>2</sub> to enhance oil and gas recovery (EOR) and storage in deep saline formations. Injecting the CO<sub>2</sub> underground involves basically the same techniques that have been used in the oil and gas exploration over the last few decades. The storage of the CO<sub>2</sub> will take place at depths below 800m, where the pressure and the temperatures are usually so high that the CO<sub>2</sub> will remain in a liquid or supercritical state.

Ocean storage, as a potential CO<sub>2</sub> sink, is still in an early research phase. The idea being that CO<sub>2</sub> will be injected directly into the ocean to depths greater than 1000m, where most of it would be isolated from the atmosphere for centuries.

Unlike CO<sub>2</sub> capture which is a proven technology with low risks, the long term effects of stored CO<sub>2</sub> can only be simulated. A lot of work in risk assessment and modelling is made to predict safe and long term storage options. [13]

### 1.1.2.3 Costs of CCS

Determination of the total costs of capture, transport and storage is really difficult and all the scenarios have a high degree of uncertainty. The major costs are in the capture and compression steps and are presently estimated to represent about 70-90% of the total CCS costs [23].

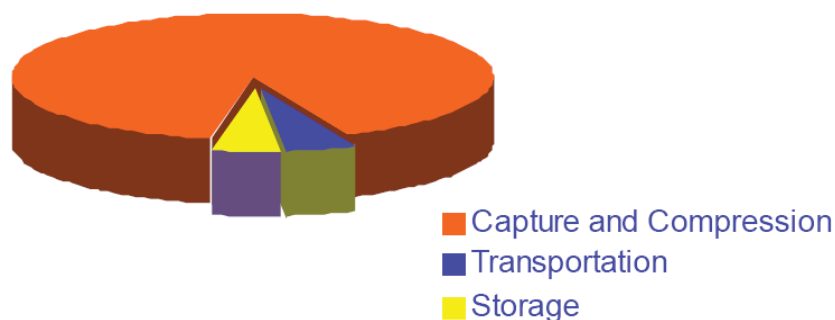


Figure 8: Composition of total CCS costs.

The costs for transport are in a range of 1 - 8 US\$/CO<sub>2,transported</sub> and strongly depended on the distance, for geological storage the cost is estimated at between 0.5 – 8 US\$/CO<sub>2,injected</sub>, whereas the captures costs are estimated to be in the range of 15 – 75 US\$/CO<sub>2,captured</sub> for coal or gas fired power plants [13].

Table 1 shows a range of the total costs for CCS based on current technologies for new power plants. Costs are given per ton CO<sub>2</sub> avoided.

Table 1: Range of total costs for CO<sub>2</sub> capture, transport and geological storage.

		Pulverized coal power plant	Natural gas combined cycle power plant	Integrated coal gasification combined cycle power plant
Increased fuel requirement	%	24 - 40	11 - 22	14 - 25
CO <sub>2</sub> avoided	%	81 -88	83 -88	81 -91
Cost of CCS	US\$/CO <sub>2</sub> avoided	30 -71	38 - 91	14 -53

## 1.2 Purpose of the Study

Pre – combustion or the Oxyfuel process are potential technologies for low emission power plants in the future. However these technologies are only serviceable if new power plants specially aligned for these technologies are built. Only post combustion can provide a solution were CO<sub>2</sub> can be captured from existing power plants, without significant modification. Also, for new power plants it is possible that post combustion is the most cost efficient solution for the capture of CO<sub>2</sub> and so a lot of research effort is currently directed into improving the performance and efficiency of this technology.

Many different solvents have been tested over the last years, especially amine and carbonate base. It turned out that amine based solvents have a slightly better performance then unpromoted carbonate solutions. The most common used solvent on amine base is MonoEthanolAmine (MEA). The absorption of CO<sub>2</sub> with MEA is effective but there are also some important limitations and problems. With time and the presence of flue gas impurities, such as SO<sub>2</sub>, NO<sub>x</sub> and O<sub>2</sub>, MEA degrades and forms a variety of substances that decrease the absorption of CO<sub>2</sub>. The capture of CO<sub>2</sub> with MEA is only possible in flue gases with low SO<sub>2</sub> concentrations because the SO<sub>2</sub> reacts with the MEA and degrades it. For European power plants where flue gas desulphurisation (FGD) is required and a proven operation, this is not a prohibitive issue as remaining SO<sub>2</sub> concentrations are not high enough to have a significant adverse affect on MEA. In Australia, the majority of the power plants do not have flue gas desulphurisation, hence this limitation is important. In such instances an additional FGD unit has to be installed to enable the use MEA as a CO<sub>2</sub> absorption solvent. This results in higher capital investment costs and opens new possibilities for carbonate based solvents such as potassium carbonate solution (K<sub>2</sub>CO<sub>3</sub>). To increase the CO<sub>2</sub> absorption performance of potassium carbonate solutions promoters are used, but these promoters are often organic or amine based and so are also susceptible to SO<sub>2</sub> degradation.

As an inorganic material, pure potassium carbonate is resistant to irreversible degradation by  $\text{SO}_2$  and in fact it is possible to capture  $\text{SO}_2$  using potassium carbonate solutions. For  $\text{NO}_x$ , another important pollutant present in flue gases, the capture using potassium carbonate is also believed to be possible.

In Europe, the standard flue gas treatment in power plants (especially coal fired power plants) has a  $\text{SO}_2$  and  $\text{NO}_x$  - removal. In most processes the  $\text{SO}_2$  is precipitated out as gypsum using calcium – carbonate ( $\text{CaCO}_3$ ) as a solvent. For the  $\text{NO}_x$  – removal via reaction with ammonia ( $\text{NH}_3$ ) converts the pollutant into pure  $\text{N}_2$ . As an additional step, the absorption/desorption process for  $\text{CO}_2$  capture would follow the  $\text{SO}_2$  and  $\text{NO}_x$  removal, as shown in Figure 9.

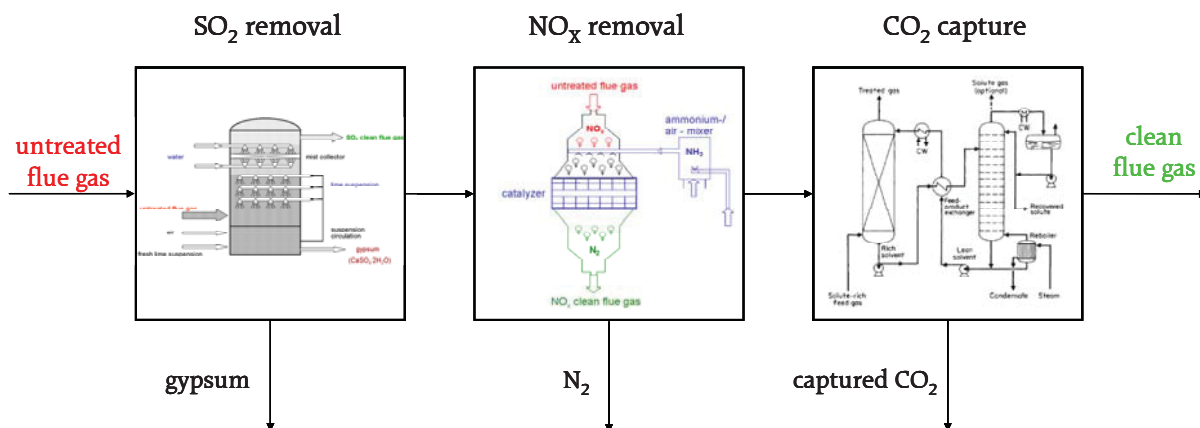


Figure 9: Multi stage flue gas treatment including  $\text{CO}_2$  capture.

This multi-stage flue gas treatment has both high capital and operating costs, however the advantage is that the technologies are proven and the efficiency is relatively high.

A possible solution to reduce capital and operating costs significantly is instead of the multi-stage flue gas treatment, the  $\text{SO}_2$ ,  $\text{NO}_x$  and  $\text{CO}_2$  are absorbed in a one process step only, as shown in Figure 10. Potassium carbonate seems to be an appropriate solvent, to absorb each of these components simultaneously. For existing power plants without advanced gas treatment, it would be a good chance to improve their emissions with relatively low investment costs compared to the standard multi-stage process. This would especially useful in Australia, where brown and black coal fired power plants with high sulphur concentrations are the main source of the energy, such a process would increase the quality of the exhaust gas significantly.

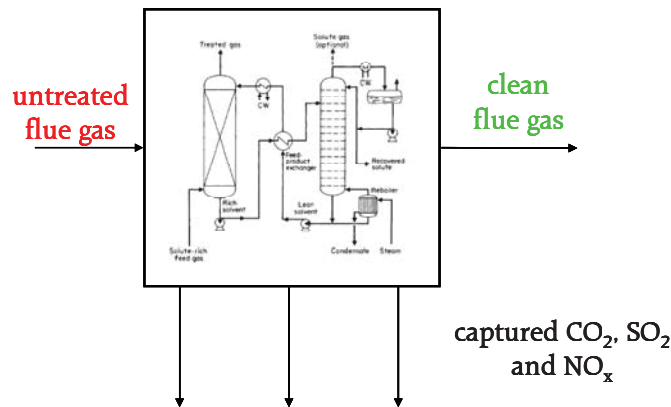


Figure 10: Single-stage SO<sub>2</sub>, NO<sub>x</sub> and CO<sub>2</sub> capture process.

The process is similar to the standard absorption/desorption process. Important for the practical viability of such a process is the further treatment of the absorbed SO<sub>2</sub> and NO<sub>x</sub>.

### 1.3 Goals of this Study

Based on the overall goal to ascertain the possible industrial use of a one step simultaneous absorption of SO<sub>2</sub>, NO<sub>x</sub> and CO<sub>2</sub>, the individual goals of this work were determined.

The main goal of this work was to investigate the effect of SO<sub>2</sub> on the equilibrium curve and absorption efficiency of carbon dioxide using 30w% of unpromoted potassium carbonate solution.

The ability to absorb a gas into a liquid is given by the vapour – liquid – equilibrium (VLE) between the gas and the solvent. The vapour – liquid – equilibrium curve expresses the relationship between the equilibrium partial pressure of the gas and the concentration of the dissolved gas in the solvent. This curve is a measurement how much of a gas can be absorbed into a solvent and one of the key issues for the design of every absorption process.

“Finding reliable gas – liquid and vapour – liquid equilibrium data may be the most time – consuming task associated with the design of absorbers and other gas – liquid contactors, and yet it may be the most important task at hand.” [2 p. 14-4]

Due to the absorption of SO<sub>2</sub> into the potassium carbonate solution, the VLE – equilibrium curve between CO<sub>2</sub> and K<sub>2</sub>CO<sub>3</sub> will change. This change can have effects on the absorption performance and efficiency of the CO<sub>2</sub> capture unit. It is important to know how the CO<sub>2</sub> equilibrium curve is changed with the absorption of SO<sub>2</sub> and how this affects the performance and efficiency of the process. A quantitative relationship between the absorbed SO<sub>2</sub> and the change of the equilibrium partial pressure shows directly this influence.

The identification of the underlying reactions and the species formed during the absorption of SO<sub>2</sub> and with that a quantitative analysis of these species, is another aspect of this work. Furthermore, investigation of the volatility and the solubility of the sulphur species in the solution will give possible methods for the removal of the dissolved SO<sub>2</sub> from the solvent.

## 2 Theoretical Part

### 2.1 Basics about Gas Absorption

#### 2.1.1 Physical Absorption

##### 2.1.1.1 Vapour Liquid Equilibrium

“At equilibrium the chemical potential of the gaseous form of substance A is equal to the chemical potential of its condensed phase.” [1, pp: 171]

The chemical potential of an ideal gas can be written as [1]:

$$\mu = \mu^0 + RT \cdot \ln\left(\frac{p}{p^0}\right) \quad (1)$$

$\mu$  = chemical potential at pressure p and temperature T  
 $\mu^0$  = standard chemical potential at pressure  $p^0$  and temperature T

To switch from the ideal to the real system, the fugacity was introduced. The chemical potential for mixtures is then [8]:

$$\mu_i = \mu_i^0 + RT \cdot \ln\left(\frac{f_i}{f_i^0}\right) \quad (2)$$

$f_i$  = fugacity of species i  
 $f_i^0$  = standard fugacity of species i

If all the phases are in equilibrium the chemical potential and resulting to that the fugacity have to be equal.

$$\begin{aligned} \mu_i^L &= \mu_i^G \\ f_i^L &= f_i^G \end{aligned} \quad (\text{for } i=1,2,3,\dots,N) \quad (3)$$

L = liquid phase  
 G = gaseous phase

The relation between the fugacity and the pressure for the liquid phase and equivalent for the gaseous phase is given by the fugacity coefficient [8]:

$$\phi_i = \frac{f_i}{x_i \cdot p} \quad (4)$$

$\Phi_i$  = fugacity coefficient of species i in liquid phase  
 $x_i$  = mole fraction of i in liquid phase  
 $p$  = total pressure

Another useful factor is the activity coefficient [2]:

$$\gamma_i = \frac{f_i}{x_i \cdot f_i^0} \quad (5)$$

$\gamma_i$  = activity coefficient of species i in solution

In practice the fugacity coefficient is used for the gaseous phase and the activity coefficient for the liquid or solid phase. For ideal conditions and low pressures, both the fugacity and the activity coefficient are equal to 1.

The equation for the equilibrium can then be expressed as:

$$f_i^L = f_i^G$$

And from Equation(4) and (5) follows that [7]:

$$\gamma_i \cdot f_i^0 \cdot x_i = \phi_i \cdot y_i \cdot p \quad (6)$$

The fugacity coefficient can be calculated using the Virial or cubic equations of state, which describe PVT behaviour of fluids (gases or liquid). The more common equations are the Van der Waals – Equation, the Soave – Redlich – Kwong – Equation (SRK) and the Peng – Robinson – Equation (PR). The activity coefficient can be calculated using the free excess Gibbs energy and for unsymmetrical activity coefficient with the extensions of the Debye – Hückel – Theory. The exact calculations of the fugacity and the activity coefficient will not be explained in this work (see Literature [7] or [8]).

For the standard fugacity  $f_i^0$  used in Equation(5) two different approaches are typically used:

1.  $f_i^0$  is the fugacity of the pure liquid at pressure p and temperature T [8]

$$f_i^0(p_i^s) = \phi_i^s \cdot p_i^s \quad (7)$$

$p_i^s$  = saturation vapour pressure of species i [kPa]



The solution of this equation is [8]:

$$f_i^0 = \phi_i^S \cdot p_i^S \cdot Poy_i \quad (8)$$

$Poy_i$  = Poynting – Factor

For most practical applications the exact solution is not required, so the simplified expression is:

$$f_i^0 = p_i^S \quad (9)$$

2.  $f_i^0$  is the Henry's constant  $H_{ij}$

Henry's constant of a soluble substance  $i$  is the slope of the fugacity for a concentration of  $x_i \rightarrow 0$  [2]

$$H_{ij} = \lim_{x_i \rightarrow 0} \frac{f_i}{x_i} \quad (10)$$

$$f_i^0 = H_{ij} \quad (11)$$

For these two approaches the equilibrium equations for the liquid phase are according to Equations(5) and (8) [8]:

$$f_i = x_i \cdot \gamma_i \cdot \phi_i^S \cdot p_i^S \cdot Poy_i \quad (12)$$

And according to Equations(5) and (11):

$$f_i = x_i \cdot \gamma_i^* \cdot H_{ij} \quad (13)$$

$\gamma_i^*$  = unsymmetrical activity coefficient

For the gas phase results from Equation(4):

$$f_i = y_i \cdot \phi_i \cdot p \quad (14)$$

If the gas and the liquid phase are ideal the simplification results in Raoult's and Henry's Law.

Raoult's Law:

$$p_i^* = x_i \cdot p_i^s \quad (15)$$

$p_i^*$  = equilibrium partial pressure of species  $i$  [kPa]

Henry's Law:

$$p_i^* = x_i \cdot H_{ij} \quad (16)$$

The relationship between the partial pressure and the mole fraction of the soluble ideal gas is given by Dalton's Law.

$$p_i^* = y_i \cdot p \quad (17)$$

Nearly pure solvents ( $x_i \rightarrow 1$ ) obey Raoult's Law, hence the vapour pressure is proportional to the mole fraction with a slope  $p_i^s$ . For the solute, with a concentration  $x_i \rightarrow 0$  the vapour pressure is proportional to the mole fraction times the Henry constant (Henry's Law). Such mixtures are called ideal – dilute solutions.

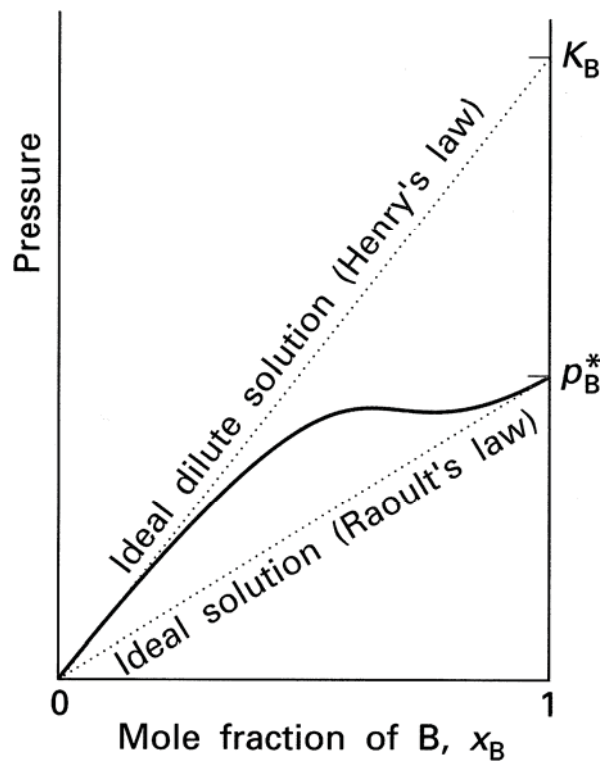


Figure 11: Raoult's Law, Henry's Law and real performance of a species  $i$  in solution [1].

### 2.1.1.2 Two Film Theory

The local mass transfer between a gas and a liquid phase is described by the two film theory from Whitman and Lewis [5]. It is based on the assumption that there is a thin film between the gas and the liquid phase where the transfer proceeds through molecular diffusion. There is no resistance at the interface between those two phases, the resistance is only in the bulk gas and liquid phases. As a result the gas and the liquid phase are in equilibrium at the interface that is they have the same chemical potential. In the thin film interface fluid the flow is strictly laminar, outside the film region the fluid flow is completely turbulent. In the turbulent flow region the solute concentration is uniform and no concentration gradient exists. However, a mass transfer gradient exists in the thin interface layer between the gas and liquid phases. According to Fick's Law the rate of mass transfer by diffusion in the laminar flow region is proportional to the concentration gradient and the interfacial area. Fick's Law is only valid for low solute concentrations, as for such systems the gradient is a straight line. For higher concentrations the gradient is curved according Stephans law [3],[5],[6].

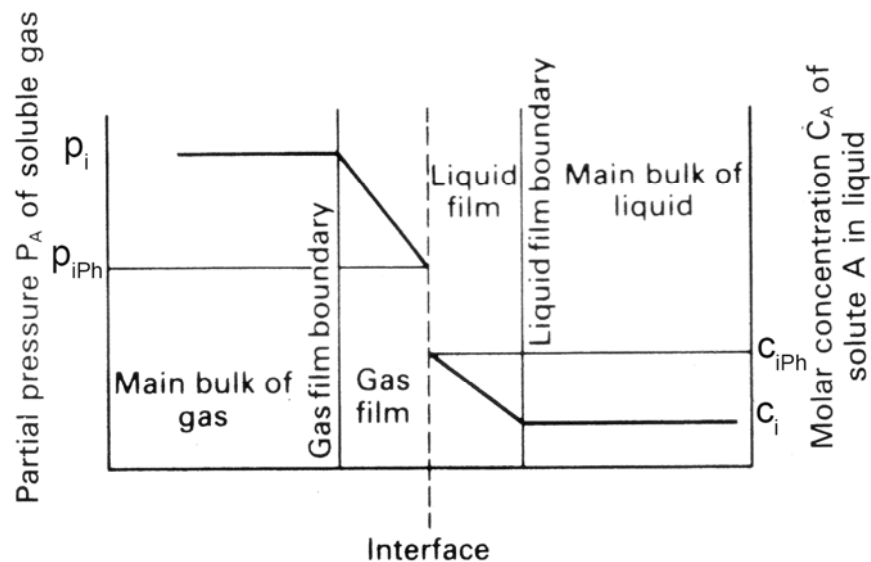


Figure 12: Concentration profile for absorbed component A [5].

The specific mass transfer through the thin interfacial layer can be described by the following expression [2]:

$$n_A = k_G \cdot (p_i - p_{iPh}) = k_L \cdot (c_{iPh} - c_i) \quad (18)$$

or alternatively [2]

$$n_A = k_G \cdot (y_i - y_{iPh}) = k_L \cdot (x_{iPh} - x_i) \quad (19)$$

$n_A$	=	specific mass transfer rate	[kmol/(s*m <sup>2</sup> )]
$k_G$	=	gas – phase mass transfer coefficient	[kmol/(s*m <sup>2</sup> )]



$k_G'$	=	gas – phase mass transfer coefficient	$[\text{kmol}/(\text{s}\cdot\text{m}^2\cdot\text{kPa})]$
$p_i$	=	solute partial pressure in bulk gas	$[\text{kPa}]$
$p_{iPh}$	=	solute partial pressure at the interface	$[\text{kPa}]$
$k_L$	=	liquid – phase mass transfer coefficient	$[\text{kmol}/(\text{s}\cdot\text{m}^2)]$
$k_L'$	=	liquid – phase mass transfer coefficient	$[\text{kmol}/(\text{s}\cdot\text{m}^2\cdot\text{kmol}/\text{m}^3)]$
$C_i$	=	solute concentration in bulk liquid	$[\text{kmol}/\text{m}^3]$
$C_{iPh}$	=	solute concentration in liquid at interface	$[\text{kmol}/\text{m}^3]$
$y_i$	=	mole fraction solute in bulk gas phase	$[\text{kmol}_{\text{solute}}/\text{kmol}_{\text{gas}}]$
$y_{iPh}$	=	mole fraction solute in gas at interface	$[\text{kmol}_{\text{solute}}/\text{kmol}_{\text{gas}}]$
$x_{iPh}$	=	mole fraction solute in bulk liquid phase	$[\text{kmol}_{\text{solute}}/\text{kmol}_{\text{liquid}}]$
$x_i$	=	mole fraction solute in liquid at interface	$[\text{kmol}_{\text{solute}}/\text{kmol}_{\text{liquid}}]$

The differences in molar concentration  $\Delta y$  and  $\Delta x$  are the driving force for mass transfer. The mass transfer gradient is then [3]

$$m = -\frac{k_L}{k_G} = \frac{y_i - y_{iPh}}{x_i - x_{iPh}} \quad (20)$$

In practice it is nearly impossible to determinate the solute concentration at the interface. This is because the layer is so thin that no samples of the layer can be taken.

Due to the fact that the equilibrium distribution curve is unique at fixed temperature and pressure, the vapour composition  $y_i^*$  in equilibrium with the bulk liquid concentration  $x_i$  is proportional to the interfacial concentration  $x_{iPh}$ . If the equilibrium relation  $y_i^* = f(x_i)$  is sufficiently simple, such as for ideal diluted solutions,  $y_i^*$  can be calculated using Henry's Law and it is not necessary to solve for the interfacial composition.

The overall rate of mass transfer can then be defined as [2]:

$$n_A = K_G \cdot (y_i - y_i^*) = K_L \cdot (x_i^* - x_i) \quad (21)$$

$K_G$	=	overall gas – phase mass transfer coefficient
$K_L$	=	overall liquid – phase mass transfer coefficient
$y_i^*$	=	vapour composition in equilibrium with $x_i$
$x_i^*$	=	liquid composition in equilibrium with vapour of composition $y_i$

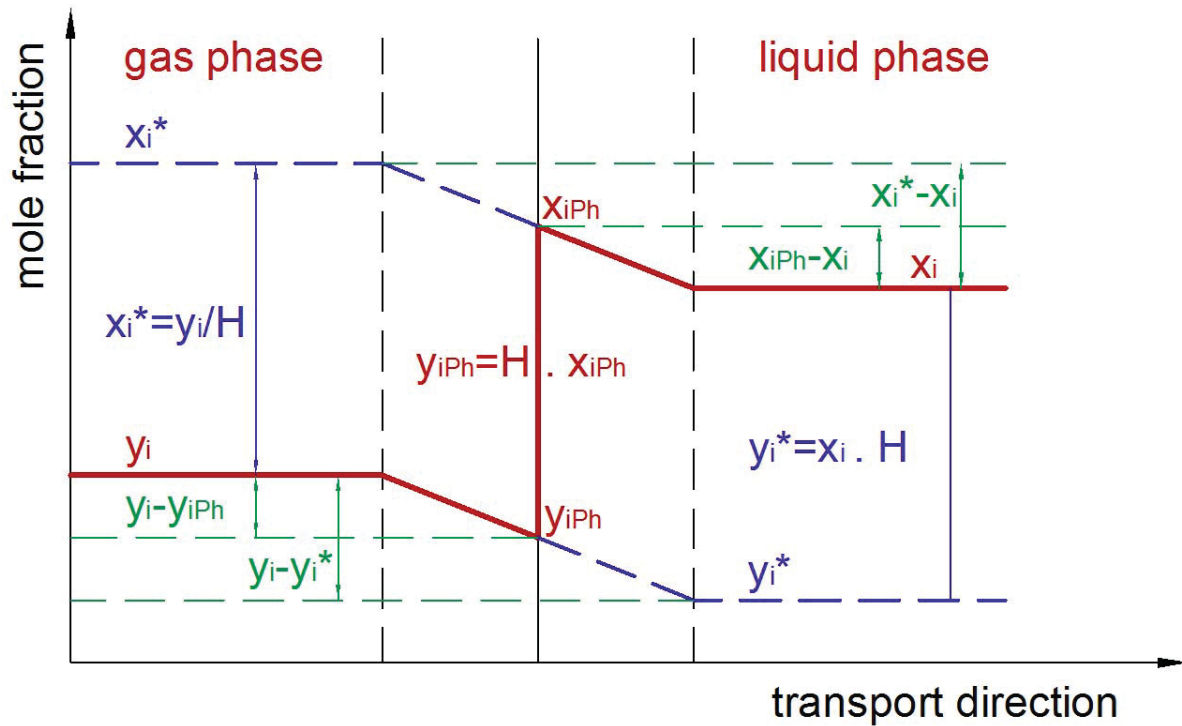


Figure 13: Driving Forces at the mass transfer.

The relationship between the overall mass transfer coefficient, and the gas and liquid phase mass transfer coefficient is given by the expression [2]

$$n_A = K_G \cdot (y_i - y_i^*) = k_G \cdot (y_i - y_{iPh}) = k_L \cdot (x_{iPh} - x_i) = K_L \cdot (x_i^* - x_i) \quad (22)$$

For the gas transfer [2], [5]:

$$\frac{1}{K_G} = \frac{1}{k_G} \cdot \frac{y_i - y_i^*}{y_i - y_{iPh}} \quad (23)$$

$$\frac{1}{k_G \cdot (y_i - y_{iPh})} = \frac{1}{k_L \cdot (x_{iPh} - x_i)} \quad (24)$$

$$\frac{1}{K_G} = \frac{1}{k_G} \cdot \frac{y_i - y_{iPh}}{y_i - y_{iPh}} + \frac{1}{k_G} \cdot \frac{y_{iPh} - y_i^*}{y_i - y_{iPh}} \quad (25)$$

$$\frac{1}{K_G} = \frac{1}{k_G} + \frac{1}{k_L} \cdot \frac{y_{iPh} - y_i^*}{x_{iPh} - x_i} \quad (26)$$

If the equilibrium curve obeys Henry's Law, the last term of the equation is equal to the slope of mass transfer as defined before [2].

$$\frac{1}{K_G} = \frac{1}{k_G} + \frac{m}{k_L} \quad (27)$$

For the liquid transfer [2], [5]:

$$\frac{1}{K_L} = \frac{1}{k_L} \cdot \frac{x_i^* - x_i}{x_{iPh} - x_i} \quad (28)$$

$$\frac{1}{K_L} = \frac{1}{k_L} \cdot \frac{x_{iPh} - x_i}{x_{iPh} - x_i} + \frac{1}{k_L} \cdot \frac{x_i^* - x_{iPh}}{x_{iPh} - x_i} \quad (29)$$

$$\frac{1}{K_L} = \frac{1}{k_L} + \frac{1}{k_G} \cdot \frac{x_i^* - x_{iPh}}{y_i - y_{iPh}} \quad (30)$$

The last term of the equation is equal to the reciprocal value of the gradient [2].

$$\frac{1}{K_L} = \frac{1}{k_L} + \frac{1}{k_G \cdot m} \quad (31)$$

These equations show that the resistance of the overall mass transfer is the sum of the individual gas and liquid phase transfer resistances.

In instance that the equilibrium line is straight that is equilibrium curve obeys Henry's Law, the relationship between gas and liquid phase overall mass transfer coefficient is [2]:

$$K_L = m \cdot K_G \quad (32)$$

When the equilibrium curve is almost horizontal ( $m \rightarrow 0$ ), the majority of substance A will be in the liquid phase that is A is very soluble in the liquid phase. As a result the factor  $1/K_G$  is the dominant resistance and the process is considered gas phase controlled. An example of such a system is  $\text{NH}_3$  in  $\text{H}_2\text{O}$ . To decrease the resistance it is important to keep the gas phase turbulent (e.g.: spray tower).

Conversely if the equilibrium curve has a steep gradient ( $m \rightarrow \infty$ ), the majority of a substance A will be in the gas phase. That is, A relatively insoluble in the liquid phase. In this case the main resistance is  $1/K_L$ , and the process is liquid phase controlled (e.g.  $\text{O}_2$  in  $\text{H}_2\text{O}$ ). For a low mass transfer resistance the liquid phase has to be turbulent, such as in bubble columns and aeration tanks [8].



The described mass transfer process is only valid locally. In practical applications the mass transfer varies from place to place because the bulk concentrations from the gas and liquid phase are not constant. According to the driving forces the variation is big for co-current flow and small for counter current flow. To get the average mass transfer over an apparatus it is either possible to determine a logarithmic average driving force or to solve the problem with integration from the inlet to the outlet concentration (HTU – NTU concept).

In most types of mass transfer unit operations the effective area for the mass transfer cannot be determined, hence the rate of transfer is generally based on per unit volume basis. This results for the overall mass transfer rate [2]:

$$\frac{1}{K_G \cdot a} = \frac{1}{k_G \cdot a} + \frac{m}{k_L \cdot a} \quad (33)$$

$$\frac{1}{K_L \cdot a} = \frac{1}{k_L \cdot a} + \frac{1}{k_G \cdot a} \cdot \frac{1}{m} \quad (34)$$

a = effective interfacial mass transfer area per unit volume [ $\text{m}^2/\text{m}^3$ ]

## 2.1.2 Chemical Absorption

Mainly commercial gas absorption processes such as absorption of  $\text{CO}_2$  in aqueous solutions, involve both physical and chemical absorption. Following mass transfer from the gas phase to the liquid phase, a chemical reaction takes place. This reaction normally enhances the rate of absorption and increases the capacity of the liquid phase to dissolve the solute in comparison to physical absorption [2],[11].

### 2.1.2.1 Chemical Absorption of $\text{CO}_2$ in Alkaline Solutions

#### 2.1.2.1.1 Mechanism of $\text{CO}_2$ Absorption

Due to the fact that  $\text{CO}_2$  is an acid gas, any alkaline solution is eligible as a chemical solvent for its absorption. In practice aqueous solutions of alkaline are used to absorb  $\text{CO}_2$ .

For all aqueous alkaline solutions the basic chemical reactions with  $\text{CO}_2$  are [18][19]:



The equilibrium constants for these reactions at 30°C are [18]:

$$K_1 = \frac{[\text{HCO}_3^-]}{[\text{CO}_2] \cdot [\text{OH}^-]} = 3.2 \cdot 10^7 \frac{\text{l}}{\text{mol}} \quad (38)$$

$$K_2 = \frac{[\text{CO}_3^{2-}]}{[\text{OH}^-] \cdot [\text{HCO}_3^-]} = 3.5 \cdot 10^3 \frac{\text{l}}{\text{mol}} \quad (39)$$

$$K_w = [\text{H}^+] \cdot [\text{OH}^-] = 10^{-14} \quad (40)$$

$K_1$  = equilibrium constant of Equation (35)  
 $K_2$  = equilibrium constant of Equation (36)  
 $K_w$  = equilibrium constant of Equation (37)

Equation (36) and (37) have very high rate constants, hence these equations can be regarded as instantaneous reversible reactions. This implies that the reaction is in equilibrium all the time.

The formation of bicarbonate, Equation(35), is practically an irreversible second order reaction that is first order with respect to both  $[\text{CO}_2]$  and  $[\text{OH}^-]$ .

The rate of reaction for the bicarbonate formation is given by the following equations [11]:

$$r = k \cdot [\text{OH}^-] \cdot ([\text{CO}_2] - [\overline{\text{CO}_2}]) \quad (41)$$

$$[\overline{\text{CO}_2}] = \frac{[\text{HCO}_3^-]}{[\text{OH}^-] \cdot K_1} \quad (42)$$

$r$  = rate of reaction [mol/(l\*sec)]  
 $k$  = reaction rate constant

The reaction rate constant for this reaction over the temperature range 0°C – 110°C can be calculated using Equation(43) [11]:

$$\log(k) = 13,635 - \frac{2895}{T} + 0,08 \cdot I_i \quad (43)$$

$I_i$  = Ionic strength

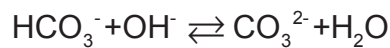
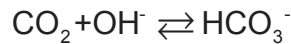
In carbonate – bicarbonate solutions the formation of  $[\text{OH}^-]$  ions, which are necessary for the chemical absorption of the  $\text{CO}_2$ , takes place via the reversible instantaneous reaction described by Equation(36).



The overall reaction of chemical CO<sub>2</sub> absorption in alkaline solutions is given by the addition of Equation(35) and (36):



According to the paper of Hikita [29] the absorption of CO<sub>2</sub> in carbonate solutions is accomplished via a two step reaction process, the irreversible second order Reaction (35) and the instantaneously reversible Reaction (36) [18],[19].



During the CO<sub>2</sub> absorption / desorption process, the alkaline carbonate solution behaves as a buffer solution, thereby maintaining the pH at a high value.

For the determination of the equilibrium partial pressure, the molarity and the degree of saturation, in further use also called solvent loading, are introduced.

“By molarity *m* the total equivalent concentration of species that may react equimolarly with component A is intended.” [11, pp: 65]

The degree of saturation *y* is defined as follows:

“*y**m* is the total concentration of chemically combined A in the liquid phase. The variable *y* takes values that may range between zero and unity if the molarity *m* has been defined appropriately.” [11, pp: 65]

For the carbonate system the molarity and the degree of saturation are defined as: [11]

$$m = [\text{CO}_3^{2-}] + \frac{1}{2} \cdot [\text{HCO}_3^-] \quad (47)$$

$$y \cdot m = \frac{[\text{HCO}_3^-]}{2} \quad (48)$$

Hence the degree of saturation, or solvent loading is then:



$$y = \frac{[\text{HCO}_3^-]}{2 \cdot [\text{CO}_3^{2-}] + [\text{HCO}_3^-]} \quad (49)$$

The equilibrium constant of the overall CO<sub>2</sub> absorption reaction (Equation(44)) can be calculated for 30°C from the individual equilibrium constants from literature by dividing Equation(38) through Equation(39). At the temperatures of 90°C and 100°C, the overall equilibrium constants were obtained from the simulation of ASPEN PLUS, where the equations for the individual reactions Equation(50) and (51) were given:



The individual equilibrium constants are given as a function of temperature in the form:

$$\ln(K_i) = A + \frac{B}{T} + C \cdot \ln(T) + D \cdot T \quad (52)$$

The equilibrium constant of the overall reaction (Equation (44)) is then given by:

$$K = \frac{K_2}{K_1} \quad (53)$$

K = equilibrium constant of the overall Reaction (44)

Table 2 shows the equilibrium constants for the absorption reaction of CO<sub>2</sub> in K<sub>2</sub>CO<sub>3</sub> from literature [18] and [19] and from the simulations of the ASPEN PLUS software package. The values at 30°C fit together pretty good and also a comparison at 90°C and 100°C with a diagram in the paper of Savage [19] shows a good compliance.

Table 2: Equilibrium constants for the absorption of CO<sub>2</sub> in K<sub>2</sub>CO<sub>3</sub>.

	30°C	90°C	100°C
<b>Literature: Hikita</b>	9142		
<b>Literature: Savage</b>		~6200	~5800
<b>ASPEN PLUS Simulation</b>	9031	5935	5588

### 2.1.2.2 Chemical Absorption of Sulphur Dioxide in Alkaline Solutions

Sulphur dioxide is absorbed into a potassium carbonate solution by the following reaction [5]



As shown, sulphur dioxide reacts with carbonate to form both sulphite and  $\text{CO}_2$ . The carbon dioxide subsequently reacts according Equation (44) resulting in the formation of bicarbonate.



If it is possible for sulphite to react further with sulphur dioxide, bisulphite is formed



The maximum amount of  $\text{SO}_2$  per mol of potassium carbonate is realised if both reactions (54) and (56) occur.

If oxygen or any other oxidant is present, the sulphite can partially react to sulphate



## 2.2 The Gas Absorption Process

“Gas absorption is a unit operation in which soluble components of a gas mixture are dissolved in a liquid. The inverse operation, called stripping or desorption, is employed when it is desired to transfer volatile components from a liquid mixture into a gas.” [2, pp: 14-4]

### 2.2.1 Equipment and Design Parameters

The most commonly used equipment for absorption and stripping unit operation are vertical cylindrical columns or towers. These units are typically filled with internal elements such as plates or packing, to enhance mass transfer performance. According to the better efficiency, the gas and the liquid flow are counter-current and the devices increase the interfacial surface, through which the mass transfer takes place. As the total interfacial surface area is directly proportional to the mass transfer, plates or packing elements should be selected to provide optimal specific surface area.

For the design of appropriate gas absorption equipment there are three basic requirements or steps [2]:

- Vapour – Liquid equilibrium data for the system



- Determination of the required height of the absorption column, including the height of a transfer unit, plate efficiency, theoretical number of transfer units, ...
- Details of the liquid and gas handling capacity device, including pressure drop, mechanic design, optimum balance between energy requirements and capital costs

Perry's Chemical Engineers' Handbook suggests that for the design of an absorption column the following parameters are important and need to be determined:

“

1. The best solvent
2. The best gas velocity through the absorber, namely the vessel diameter
3. The height of the vessel and its internal members, which is the height and type of packing or the number of contacting trays
4. The optimum solvent circulation through the absorber and stripper
5. The temperatures of streams entering and leaving the absorber and the quantity of heat to be removed to account for heat of solution and other thermal effects
6. The pressures at which the absorber and the stripper will operate
7. The mechanical design of the absorption and stripping vessels (normally columns or towers), including flow distributors, packing support and so on. “ [2, p: 14-5]

The selection of the solvent and with that the solubility of the gas in the liquid, is one of the most critical steps of the design and operation parameters. Inherently it is preferred that the gas has a high solubility in the liquid phase. Other important parameters include the cost, the solvent volatility, the corrosivity, the viscosity, the foaming properties etc.

The solubility of the gas component can be expressed as the vapour pressure of the pure component over a specific solution. For the complete specification of the solubility three key parameters are required:

- Temperature of the system
- Equilibrium partial pressure of the soluble gas component in the gas phase
- Concentration of the soluble gas component in the liquid phase

For low pressure systems ( $p_{\text{tot}} < 5 \text{ atm}$ ), such as the treatment of the flue gas streams, the partial pressure is relatively independent of the total pressure of the system.



The stripping process, the reverse of absorption, has the aim to remove the absorbed gas component from the liquid by heating and contacting with another gas stream. For the majority of industrial applications water vapour is used as the stripping gas.

To alter the equilibrium position and with that the solubility of the absorbed gas, the pressure or temperature has to be changed during the stripping process. The solubility and hence absorption of gas in a liquid increases with higher pressure and decreases with higher temperature. Hence for stripping the pressure is typically decreased and the temperature increased.

### 2.2.2 Flow Sheet and Mode of Operation

A typical flow sheet for an absorption and stripping process is shown in Figure 14 [2]:

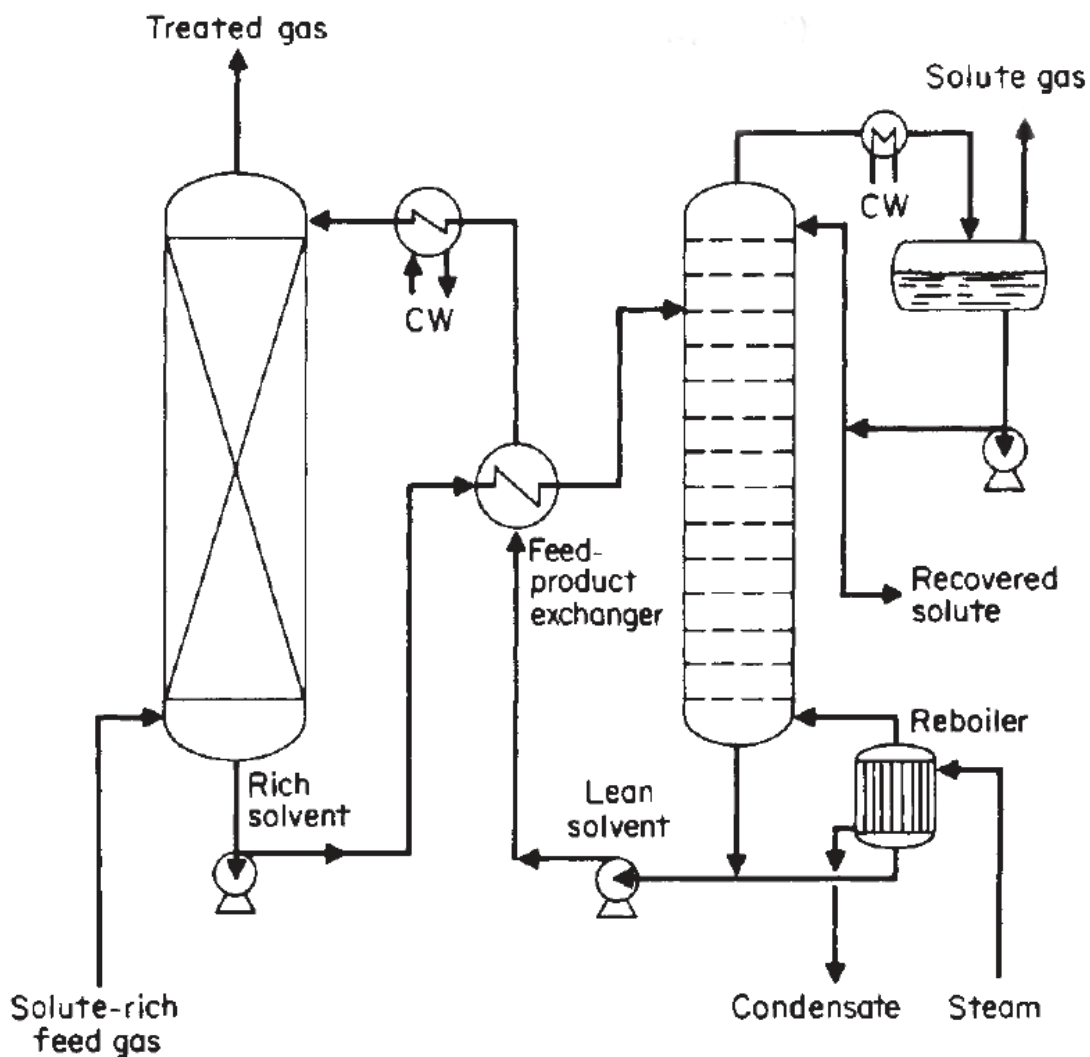


Figure 14: Gas absorber using a solvent regenerated by stripping.

The untreated feed gas enters the absorption tower at the base and is contacted with the solvent in a counter-current flow arrangement. For industrial CO<sub>2</sub> absorption the solvent may be either an amine such as MEA or DEA or an alkaline – carbonate such as potassium carbonate with or without promoter. During the pass through of the absorber the solute gas is absorbed from the gas stream into the liquid phase according to the vapour – liquid equilibrium curve. The counter – current flow arrangement in the column provides a relatively constant solute concentration difference and hence driving force for mass transfer between the gas and the liquid phases. It is assumed that however the gas and the liquid phases are in equilibrium over the whole column. The solute lean treated gas is removed from the top of the column, while the loaded or rich solvent, with an increased concentration of the solute gas, is drawn off at the absorber. Gas absorption processes are exothermic, consequently the temperature in the base of the absorber column may increase slightly from the top to the base. The loaded rich solvent is then pumped to the top of the stripper through a heat exchanger. The heat exchanger is used to preheat the solution to enhance the stripping performance of the solute gas and reduce the reboiler heat duty. Only an increase in temperature or decreasing of the pressure, does not give adequate solvent regeneration. The stripping process is usually accomplished with steam that is generated in the stripper reboiler and enters the column at the base. The steam vaporizes the solute gas from the solvent. The solute gas rich vapour stream leaving the top of the stripper is passed through a condenser where excess water is condensed out and a relatively pure captured solute gas stream is obtained. The necessary heat for the vaporization of the water added in the preheater and reboiler, is removed from the system in the condenser. The condensed water can be feed back to the stripper. The regenerated absorption solvent drawn from the base of the stripper, is pumped back via several heat exchangers, where it is cooled down to enhance the absorption performance and enhance heat recovery to the absorption column.

### 2.2.3 Absorption and Stripping Diagrams

For the determination of the concentrations of the various liquid and gas phase components and the liquid and vapour stream flows, the diagrams seen in Figure 15 and Figure 16 are particularly useful [2]:



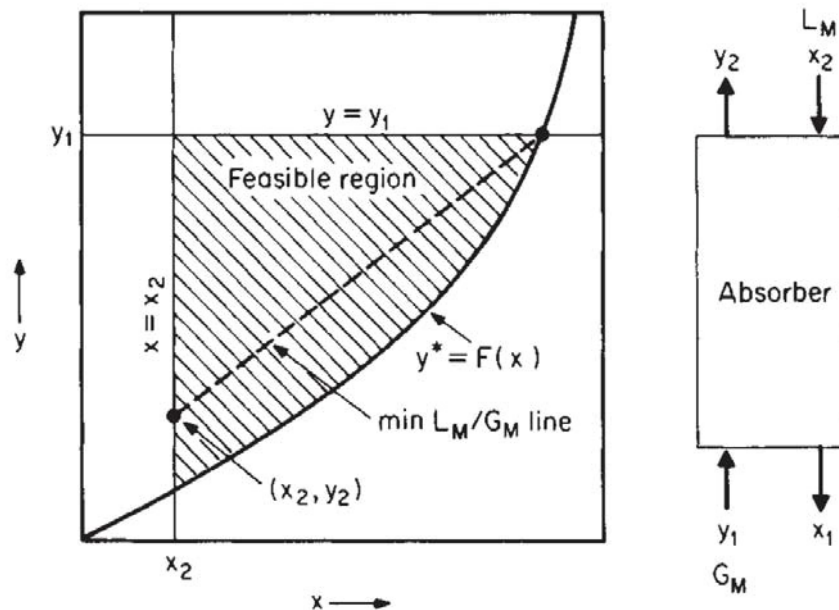


Figure 15: Design diagrams for absorption.

In both diagrams Figure 15 for absorption and Figure 16 for stripping, the  $x$  – axis represents the molar fraction of the solute in the liquid phase ( $x$ ) and the  $y$  – axis the molar fraction of the solute in the gas phase ( $y$ ).

As mentioned earlier, the most important data set for the design of an absorber or stripper is the equilibrium curve. For an ideal gas phase the concentration  $y$  can be calculated from the partial pressure with Dalton's Law refer Equation(17). In general absorption applications the inlet composition of the liquid stream and the inlet composition of the gas stream are known. The outlet solute concentration of the gas stream is the value which has to be achieved. In many applications this level is set by environmental law and the inlet solute concentration of the solvent is identical to the outlet solute concentration of the stripper. For ideal conditions this concentration is zero. These two values yield the point  $(x_2, y_2)$ . The theoretical minimum liquid – to – gas ratio ( $L_M/G_M$ ) is determined by connecting this point with the intersection of the horizontal line  $y=y_1$ , given by the inlet solute concentration of the gas stream and the equilibrium curve. This line is called the operating line, the slope of this line corresponds to the theoretical minimum liquid – to - gas ratio. The actual design value  $L_M/G_M$  for gas absorption of should be around 1.2 – 1.5 times this minimum [2]. The actual liquid – to – gas ratio the point  $(x_1, y_1)$  is shifted to the left along the line  $y=y_1$ .

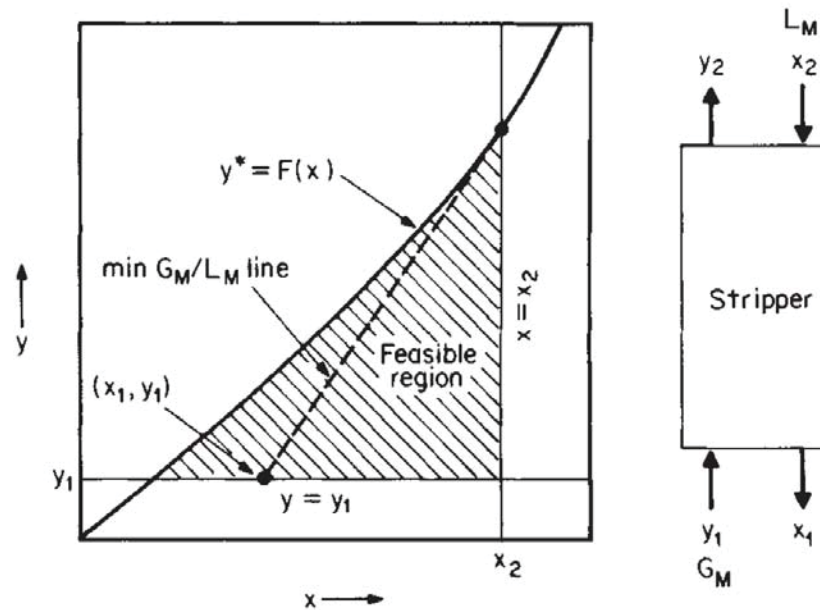


Figure 16: Design diagrams for stripping.

During stripping the operating line is below the equilibrium curve. For the design of a stripper, first the point  $(y_1, x_1)$  in Figure 16 with the outlet solute concentration of the solvent, identically with  $x_2$  from the absorption diagram according to Figure 15 and for ideally conditions equal to zero, and the inlet concentration of the water vapour stream (ideally also zero) has to be located. The theoretical minimum gas – to – liquid ratio ( $G_M/L_M$ ) is defined as the intersection of the vertical line  $x=x_2$ , inlet solute concentration of the liquid which is equivalent to the outlet concentration of the loaded solvent from the absorption process, with the equilibrium curve. As for the absorber, the slope determines the theoretical minimum gas – to – liquid ratio for stripping. Typically the values of gas absorption are about 20 to 50 percent higher than the Minimum [2], which shifts the actual operation point down along the line  $x=x_2$ .

In both diagrams the hatched area indicates the feasible region for the operation line. With increasing of the liquid – to – gas ratio (or the gas – to – liquid ratio for stripping) the amount of the theoretical stages decreases but the flow of the liquid (or stripping steam) increases. The first theoretical endpoint is given by the minimum liquid – to – gas ratio (or the gas – to – liquid ratio for stripping), where the flow stream gets to a Minimum, with an infinite number of theoretical stages. The second endpoint shows only one theoretical stage but the flow rate of the liquid (or stripping steam) gets infinitely high. Based on the operation and installation costs the best ratio can be determined.

To calculate the height of the absorption or stripping column the mass transfer at the gas – liquid interface has to be determined (See Section: 2.1.1.2). A quite common method is the NTU – HTU concept, more accurate information can be obtained from [2], [5], [8].

## 2.3 Alkali – Metals (Potassium Carbonate) as an Absorption Medium

### 2.3.1 CO<sub>2</sub> Absorption with Potassium Carbonate

#### 2.3.1.1 Properties of the Aqueous Potassium Carbonate Solution

A key factor of the absorption efficiency of CO<sub>2</sub> of the aqueous potassium carbonate solution is dependent on the potassium carbonate concentration in the solution. The effect of the temperature and percentage conversion to bicarbonate on the solubility of the salts in the system is shown of Figure 17. [4]

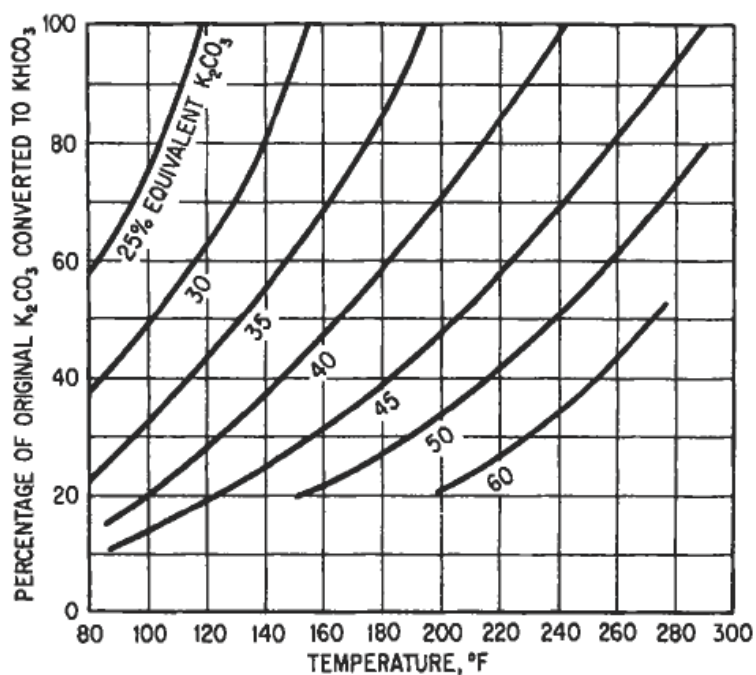


Figure 17: Effect of temperature and percentage conversion to bicarbonate on solubility of K<sub>2</sub>CO<sub>3</sub> plus KHCO<sub>3</sub>.

The lines indicate the conditions under which potassium bicarbonate begins to precipitate out. For example the 60% carbonate solution can only be converted to approximately 25% bicarbonate at a temperature of 110°C (230°F), after which bicarbonate starts to precipitate out. Theoretically the K<sub>2</sub>CO<sub>3</sub> of a 45% solution can be completely converted to KHCO<sub>3</sub> at a temperature of 145°C (290°F). Under typical conditions a 40% K<sub>2</sub>CO<sub>3</sub> solution is the maximum that can be practically used for most industrial processes. Even so practical 30% K<sub>2</sub>CO<sub>3</sub> solution is a design value for most applications. It is essentially that the process conditions are maintained such that complete solubility of the carbonate – bicarbonate maintained.

### 2.3.1.2 Hot Potassium Carbonate (Benfield) Process

The hot potassium carbonate process, also called the Benfield process, is the most common and industrially proven process for the absorption of  $\text{CO}_2$  using potassium carbonate as the solvent. It is based on the difference in the solubility of  $\text{CO}_2$  at the high partial pressure conditions in the absorber and at low partial pressure conditions of the stripper. The process was originally developed by the U.S. Bureau of Mines in 1954 to reduce the costs of synthesis – gas purification for the production of liquid fuel from coal. The process was designed to optimally utilise the synthesis – gas process stream conditions that is high temperatures and high partial pressures. Due to the high temperature in the absorber, it is not necessary to further heat the solution to the stripping temperature using steam generated in the stripping process. This results in a lower process energy requirement and eliminates the need for heat – exchange equipment between the absorber and the stripper columns. Furthermore, the operation at such high temperatures increases the solubility of the bicarbonate species, so the Benfield process can operate with highly concentrated solutions.

Over the last couple of decades many improvements and variations, such as amine activators, LoHeat Benfield Process, have been made, however in this work only the basic process will be described. A typical Benfield process flowsheet with split stream is shown in Figure 18 [4]:

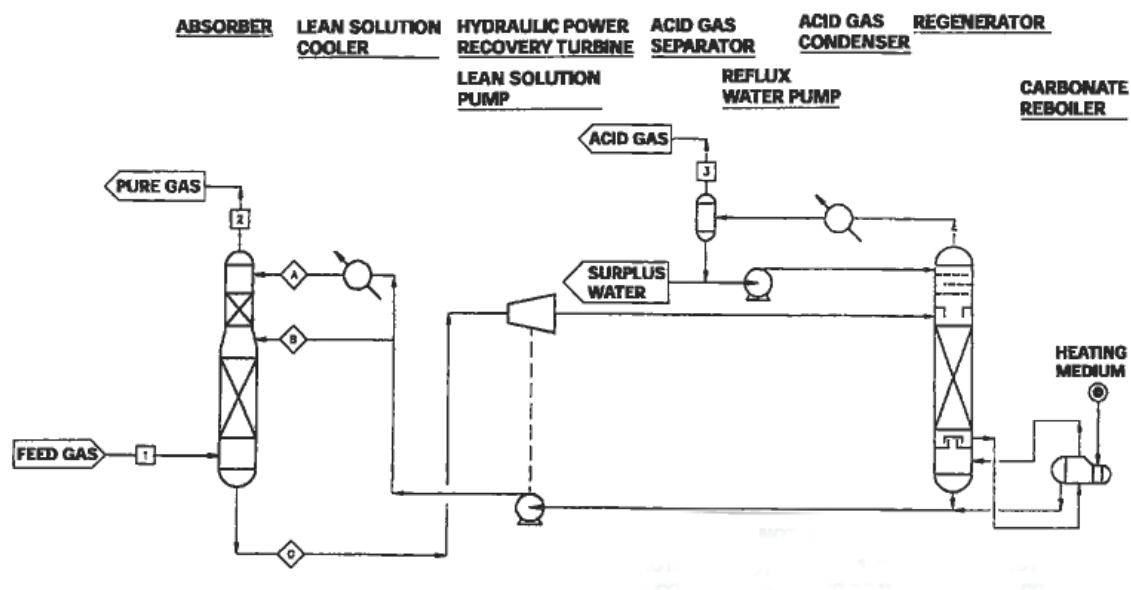


Figure 18: Flow diagram of hot potassium carbonate process with split stream.

The Benfield process basically operates like the standard gas absorption process described in Section 2.2.2. The difference between the standard absorption process and the split – stream process is that the majority of the lean solution is added hot at an intermediate stage of the absorber, while the remainder is cooled and fed directly at the top of the stage. This

slight modification improves the recovery of the solute gas by shifting the equilibrium point with lower equilibrium partial pressure of  $\text{CO}_2$  contacting with lean solution. To enhance the  $\text{CO}_2$  rich solvent stripping performance, the pressure is reduced after the absorption column with some energy recovery possible using a hydraulic power recovery turbine. To enhance the mass transfer packing is preferred over trays in the columns used for the Benfield process.

## 2.3.2 $\text{SO}_2$ Absorption with Alkali – Metals

There are a couple of industrial processes in use which use alkali – metals such as sodium (Na) or potassium (K) to absorb  $\text{SO}_2$  from flue gases. Other than the double alkali process which will be discussed in the following section, the Wellman – Lord Process is also an example of the use of alkali – metals as an absorption medium, in this case potassium [4].

### 2.3.2.1 Double Alkali Process

The basic of the double alkali process is the direct contact of the gas with a solution of soluble alkali metal, to absorb the  $\text{SO}_2$ . The reacted  $\text{SO}_2$  is subsequently precipitated as insoluble calcium sulphite and the solvent regenerated. A basic flow sheet for the double alkali process is shown in Figure 19 [4]:

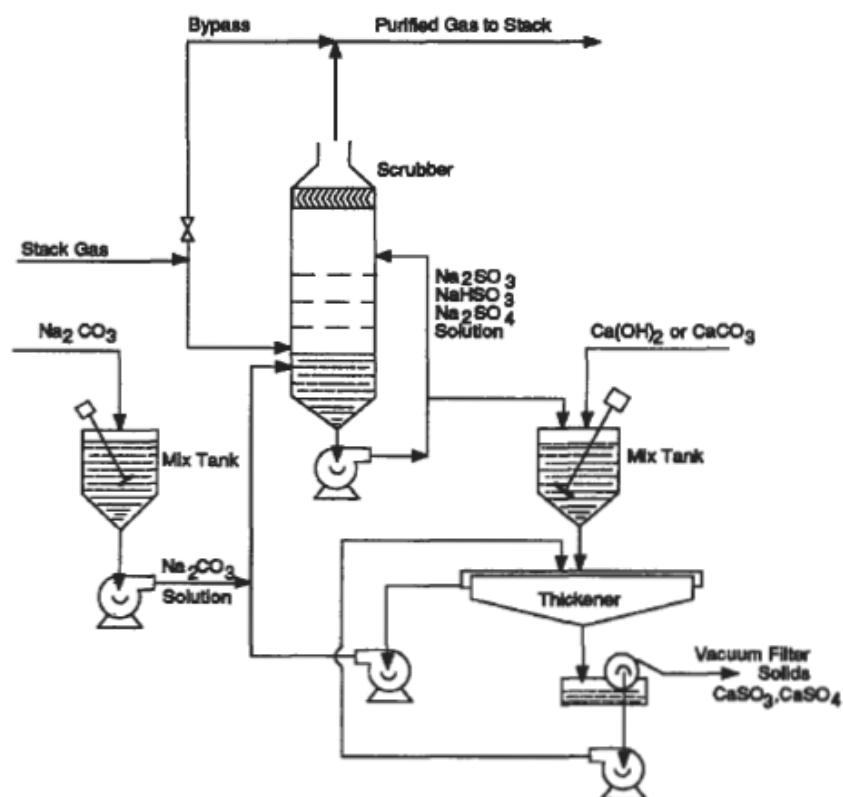


Figure 19: Flow sheet of the double alkali flue gas desulphurization process.

The sodium carbonate solution ( $\text{Na}_2\text{CO}_3$ ) absorbs  $\text{SO}_2$  according to the overall reaction:



The formed sodium sulphite ( $\text{Na}_2\text{SO}_3$ ), the principle reactive component, can be further converted to bisulphite ( $\text{NaHSO}_3$ ) by reacting with additional  $\text{SO}_2$  according the reaction:



Once the solution is loaded, a sidestream is removed and treated with lime  $\text{Ca}(\text{OH})_2$  or limestone  $\text{CaCO}_3$ . In this step, the sulphur is precipitated out as insoluble calcium sulphite and can be readily removed by settling in a thickener followed by filtration. The regenerated solution is then pumped back to the scrubber and with  $\text{Na}_2\text{CO}_3$  addition to compensate for any sodium losses.

The precipitation of the dissolved sulphur with calcium is also a possible option for the removal of sulphur from the potassium carbonate solution, following the absorption of  $\text{SO}_2$  and  $\text{CO}_2$  from brown coal flue gas.

## 3 Experimental Part

### 3.1 The Equilibrium Rig

All the equilibrium measurements were accomplished using the vapour – liquid equilibrium rig shown in Figure 20 and Figure 21. This apparatus is based on the papers of Nasir [9] and Isaacs [10], and was constructed by the University of Melbourne Chemical + Biomolecular Engineering workshop staff.

#### 3.1.1 Design and Schematic



Figure 20: Photo of the equilibrium rig.

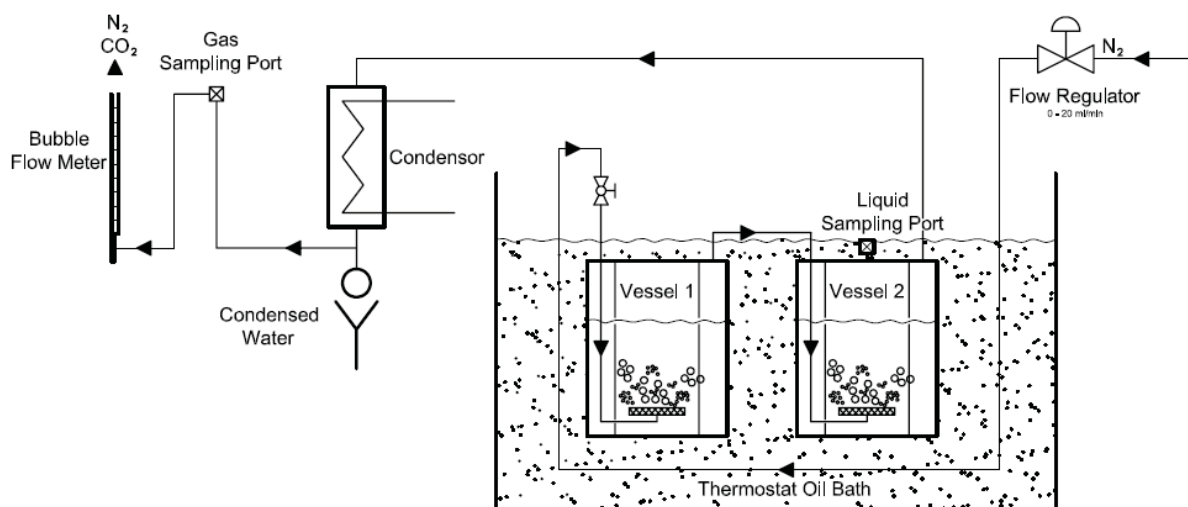


Figure 21: Schematic of the equilibrium rig.

### 3.1.2 Operation Mode

The experimental rig consists of two stainless steel vessels each with a volume of approximately 300 ml connected in series. For enhanced thermal conductivity baffle plates are provided in each vessel. The two vessels are placed in a thermostat oil bath, to maintain a constant temperature during the experiments. Due to the fact that the experimental temperatures were at 90°C and 100°C, water was not feasible as the heating medium and hence oil was used. The temperature was set using an electrical heater with a sensitivity of  $\pm 0.1^\circ\text{C}$ . However, it was assumed that during the experiments the temperature did not vary by more than 0.5°C. For better thermal equilibrium a stirrer was used in conjunction with the electrical heater.

At the start of the experiment, every vessel was filled with 200 ml of loaded potassium carbonate solution. The potassium carbonate solution had either been loaded with  $\text{CO}_2$  only or first with  $\text{SO}_2$  and subsequently with  $\text{CO}_2$ . The carrier nitrogen gas was preheated in the oil bath and then passed through each of the vessels. In each vessel a stainless steel filter (grid) element is welded to the end of a dip tube to enhance the dispersion of the nitrogen gas in the carbonate solution. During this experiment, the loaded potassium carbonate solution releases a certain amount of  $\text{CO}_2$  into the gas phase, according to the vapour liquid equilibrium, which is then carried with the inert nitrogen flow to either the second vessel or to the outlet. A really low flow rate of the nitrogen, in the range of about 5 – 10 ml/min, is required to achieve equilibrium. The flow rate can be controlled with a flow regulator between 0 and 20 ml/min, however the actual value of the flow rate is not too important for the results of the experiments. The reason for such low flow rates, as mentioned earlier is to achieve

equilibrium. At higher flow rates more  $\text{CO}_2$  is desorbed and consequently the concentration in the liquid phase continually changes with time and equilibrium is not achievable.

The gas stream outlet after the second vessel was passed through a condenser, to remove the condensable water. The gas was sampled for analyses in the gas chromatograph (GC) from a sampling point after the condenser. The gas stream leaves the system via a bubble flow meter. The bubble flow meter was used to monitor the gas flow rate which could be adjusted using the regulator at the gas inlet of the system.

The liquid sample, which was analysed by acid titration, was taken using a syringe via the sampling port located on the second vessel.

For the analysis of the gas and liquid samples, the equilibrium position had to be attained. This position was achieved when a couple of gas sample measurements over time showed a constant composition of  $\text{CO}_2$  and  $\text{N}_2$ . Normally the equilibrium position was reached after 1 hour but for all the experiments the samples were taken after at least 2 hours of runtime. At that point the actual gas and liquid samples were taken and analysed.

To calculate the  $\text{CO}_2$  partial pressure and to construct the equilibrium curve, it was also necessary to record the barometric pressure. The barometric pressure was measured using a mercury – barometer. Due to the very low gas flow rate and hence the low pressure drop in the system, it can be assumed that the barometric pressure is equal to the pressure in the second vessel.

As the whole system operates at approximately atmospheric pressure, there is a high rate of water loss from the potassium carbonate solution at temperatures above  $100^\circ\text{C}$ . Hence above  $100^\circ\text{C}$  a stable equilibrium point can not be achieved because the solution concentration in the vessels changes relatively quickly due to the vaporization of water. For measurements over  $100^\circ\text{C}$ , it is necessary for the system to be pressurized, thereby increasing the boiling point of water and creating stable conditions.

### 3.1.3 Loading of the Solutions

Each of the used potassium carbonate solutions for the equilibrium measurements were prepared and preloaded in a separate vessel. If the solution was loaded only with carbon dioxide, the  $\text{CO}_2$  was bubbled at a gas flow rate of 100 ml/min through the solution. A glass sparger was used to create smaller bubbles and hence increase the rate of  $\text{CO}_2$  absorption. For the higher solution loading the vessel was kept in a water bath at about  $60^\circ\text{C}$  to prevent precipitation of the bicarbonate species.

For the subsequent experiments with  $\text{CO}_2$  and  $\text{SO}_2$  combined loaded solutions, the potassium carbonate solution was first loaded with the  $\text{SO}_2$ . In a fume cupboard the  $\text{SO}_2$  was bubbled through the solution at room temperature. During the  $\text{SO}_2$  loading no sparger could be used due to blockages resulting from the precipitation of bicarbonate. Continuous loading



of the solution was not possible, even with a glass tube as with the sparger precipitated bicarbonate was found to block the tube. To simplify loading of carbonate solutions, a bigger volume was loaded with SO<sub>2</sub> until precipitation occurred at room temperature. Slight heating of the solution, redissolved the bicarbonate and the concentrated loaded solution was obtained. From this highly concentrated loaded solution, other solutions were prepared by diluting it with fresh potassium carbonate to give the desired concentration of dissolved sulphur. Three different sulphur concentrations were selected for the equilibrium curve experiments, were a 1:8 dilution (1 part of the highly SO<sub>2</sub> loaded solution and 8 parts of the fresh potassium carbonate solution), a 1:16 dilution and a 1:25 dilution.

For the equilibrium experiments at a certain sulphur concentration, these solutions were subsequently loaded with different concentrations of CO<sub>2</sub>. For each sulphur concentration, solutions with four different CO<sub>2</sub> loadings were prepared.

## 3.2 Analysis of Carbonate

### 3.2.1 Titration

All the liquid samples of the potassium carbonate solution were analysed for the carbonate and bicarbonate species by acid - base titration. The titrations were performed using a Metrohm – Titrand 809, the data were collected by a computer using the Metrohm tiamo software package.

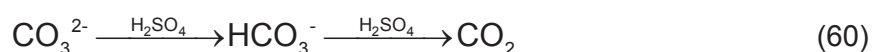
For the titrimetric determination of the carbonate and bicarbonate species concentrations a 0.4 mol/liter sulphuric acid (H<sub>2</sub>SO<sub>4</sub>) standard solution was used.

A 2 ml sample of the potassium carbonate solution was used for the solution analysis. A smaller solution sample was found to increase the error of the analysis, while a larger volume of K<sub>2</sub>CO<sub>3</sub> resulted in excessive acid consumption. This solution sample was then diluted with 20ml of deionised water.

During the titration H<sub>2</sub>SO<sub>4</sub> was continuously dosed into the stirred sample while the pH was simultaneous measured and recorded as shown by the typical curve in Figure 22. From the resulting titration curve and it's derivate the titration endpoints and hence the carbonate and bicarbonate concentrations can be calculated.

#### 3.2.1.1 Calculation of Carbonate and Bicarbonate Concentration

The addition of the acid causes the following 2 step reaction to occur in the system:



Firstly all of the carbonate species is converted to bicarbonate, when this step is complete the bicarbonate, both that initially present and that formed by the first step, is converted to CO<sub>2</sub> which is released from the sample.

When all the carbonate is consumed and converted, the first endpoint (EP 1) is achieved as shown in Figure 22. This results in a reversal point the pH curve (or a maximum in the change of the pH). By further adding acid the bicarbonate is converted to CO<sub>2</sub> and when this reaction was complete the second endpoint (EP 2) is reached. As a result another reversal point with maximum in the change of the pH is observed on the titration curve.

The carbonate and bicarbonate concentrations are calculated from the respective endpoint results using the following equations:

$$[\text{CO}_3^{2-}] = \frac{V_{\text{EP1}} \cdot c_{\text{H}_2\text{SO}_4} \cdot 2}{V_{\text{Sample}}} \quad (61)$$

$$[\text{HCO}_3^-] = \frac{(V_{\text{EP2}} - 2 \cdot V_{\text{EP1}}) \cdot c_{\text{H}_2\text{SO}_4} \cdot 2}{V_{\text{Sample}}} \quad (62)$$

[CO <sub>3</sub> <sup>2-</sup> ]	=	concentration of carbonate [mol/l]
[HCO <sub>3</sub> <sup>-</sup> ]	=	concentration of carbonate [mol/l]
V <sub>EP1</sub>	=	volume of H <sub>2</sub> SO <sub>4</sub> added until Endpoint 1 is reached [ml]
V <sub>EP2</sub>	=	volume of H <sub>2</sub> SO <sub>4</sub> added until Endpoint 2 is reached [ml]
c <sub>H2SO4</sub>	=	concentration of sulphuric acid (0.4 mol/l) [mol/l]
V <sub>Sample</sub>	=	volume of the potassium carbonate sample (2ml) [ml]

### 3.2.1.2 Diagram of a $K_2CO_3$ Titration

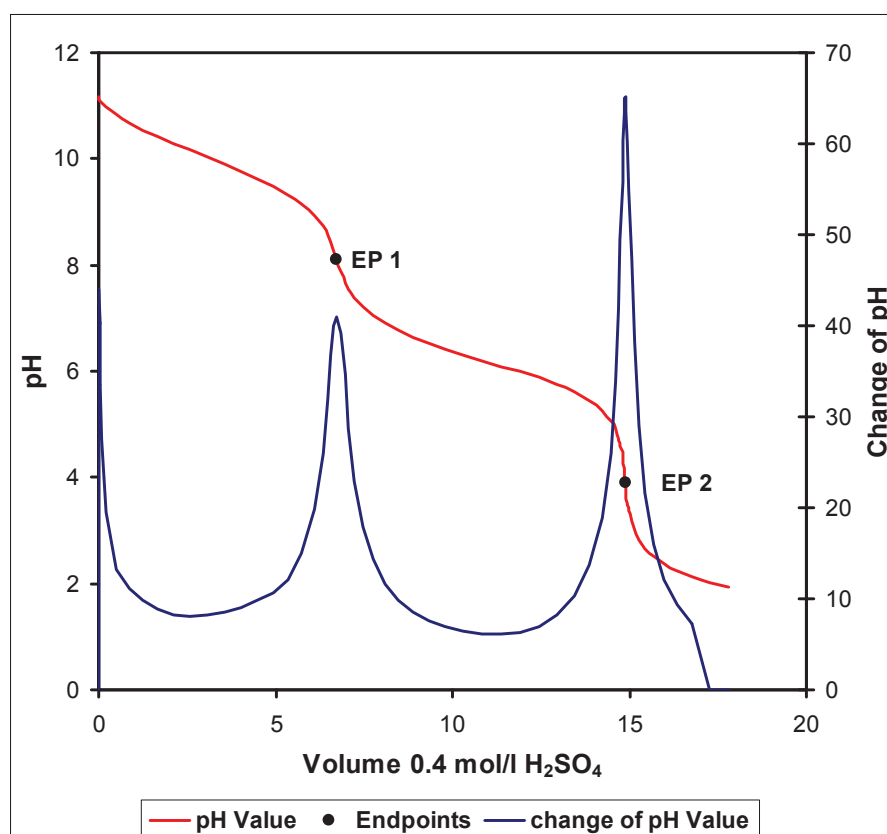


Figure 22: Typical titration curve for a loaded  $K_2CO_3$  solution.

### 3.2.2 Gas Chromatography

The analysis of the gas samples taken from the equilibrium rig was completed using a Shimadzu Gas Chromatograph GC – 8A. A stainless steel Porapak Q column with a Mesh Range of 120/100 was used to achieve the chromatographic separation of gas compounds. The total length of this column was 8 feet, the outer diameter was 1/8" and the inner diameter 0.85".

After injecting the gas sample the automatic integrator for calculating the area of the peaks was started. As the gas from the  $CO_2$  loaded solutions contained only nitrogen from the carrier gas and carbon dioxide from the carbonate solution. For the  $SO_2$  and  $CO_2$  loaded solution experiment it was possible that there was some  $SO_2$  in the sampled gas from the loaded solution. However, with the column used it was not possible to separate and detect the  $SO_2$  gas, hence the only gas components detected were nitrogen and carbon dioxide.

Different GC temperature settings were tested and optimised for the gas stream components. Settings with injection temperature of 190°C and 90°C column temperature resulted in a chromatogram with relatively flat and wide peaks. At the higher temperatures of 240°C and 120°C for the injection and column temperature respectively the peaks on the

chromatogram were sharper, higher and closer together. Typically if the peaks are sharper, it is easier to identify the start and end of the peak and with that the error of the measurement is reduced.

Other than temperature, the height of a peak is also dependant on the current setting of the temperature controlled detector (TCD). A minimum current of 70mA was used, due to the quite small peak areas at 190°C / 90°C temperature settings. For CO<sub>2</sub> concentrations this resulted in a higher experimental error compared with a 100mA current setting. At 100mA the TCD base line has more noise and hence it can be more difficult to determine the start and end of each peak.

After the detection of the peaks was completed, the start and the end of each peak detected by the area integration were adjusted manually to minimize the reading error. Automatic area integration is also possible but in many cases the right peak limits are not taken. This occurs especially when the background noise is high. In such instances the automatic integration can give misleading and incorrect results.

Due to the shape of the resulting peaks, the best GC settings for the CO<sub>2</sub> equilibrium gas samples were 240°C and 120°C for the injection and column temperature. The current should either be 80mA or 100mA. Even though there is a high level of noise at 100mA, the error it introduces is low as the peak uncertainty area at the start and end of each peak is relatively low in comparison to the total peak area. Due to the fact that the GC was also being used by other users in the laboratory, who used temperature settings of 190°C / 90°C, some of the samples were analysed using these less optimal settings.

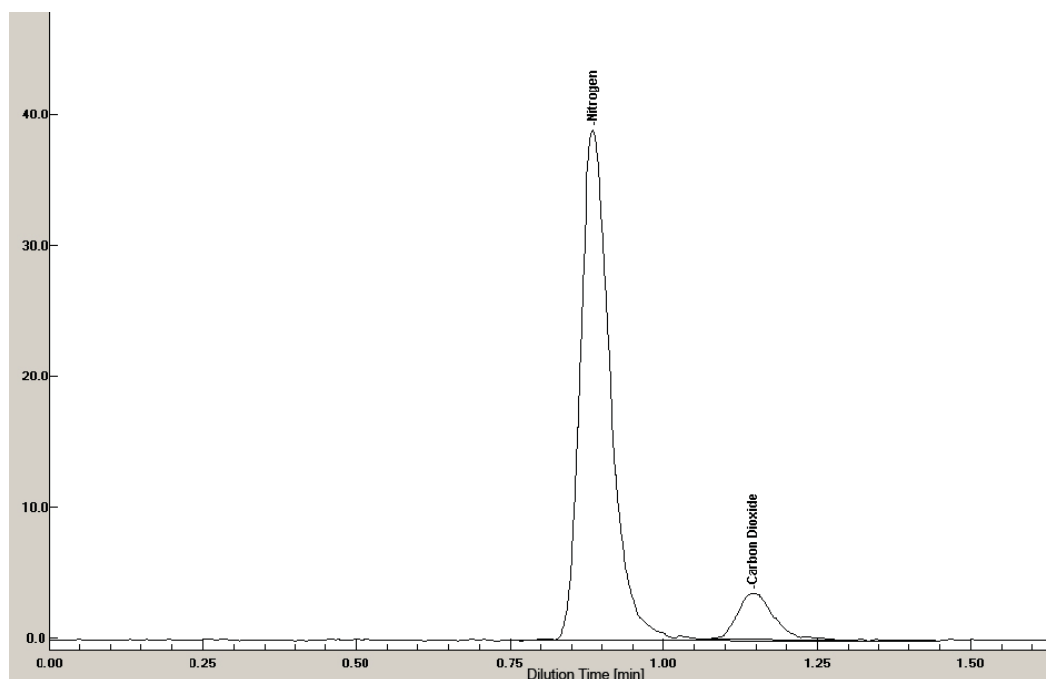


Figure 23: Typical Gas Chromatogram with peaks for N<sub>2</sub> and CO<sub>2</sub> binary gas mixtures identified.

### 3.2.2.1 The Calibration Curve

To quantify the nitrogen and carbon dioxide in the gas stream, the resulted peaks were converted into a volumetric or molar fraction of the calibration curve. Every different temperature or current settings combination requires a complete calibration curve. For each equilibrium test a new calibration curve was constructed or the accuracy of an existing curve was verified. To construct the calibration curve, specific amounts of pure N<sub>2</sub> or CO<sub>2</sub> from ultra high purity gas cylinders were injected into the gas chromatograph. The resulting peak area and injected volume were used as one point of the calibration curve. For calibration at new temperature or current settings at least three measurements were made for every injecting volume. A typical calibration curve for gas chromatography temperature settings of 240 / 120°C and a current of 100mA is shown in Figure 24.

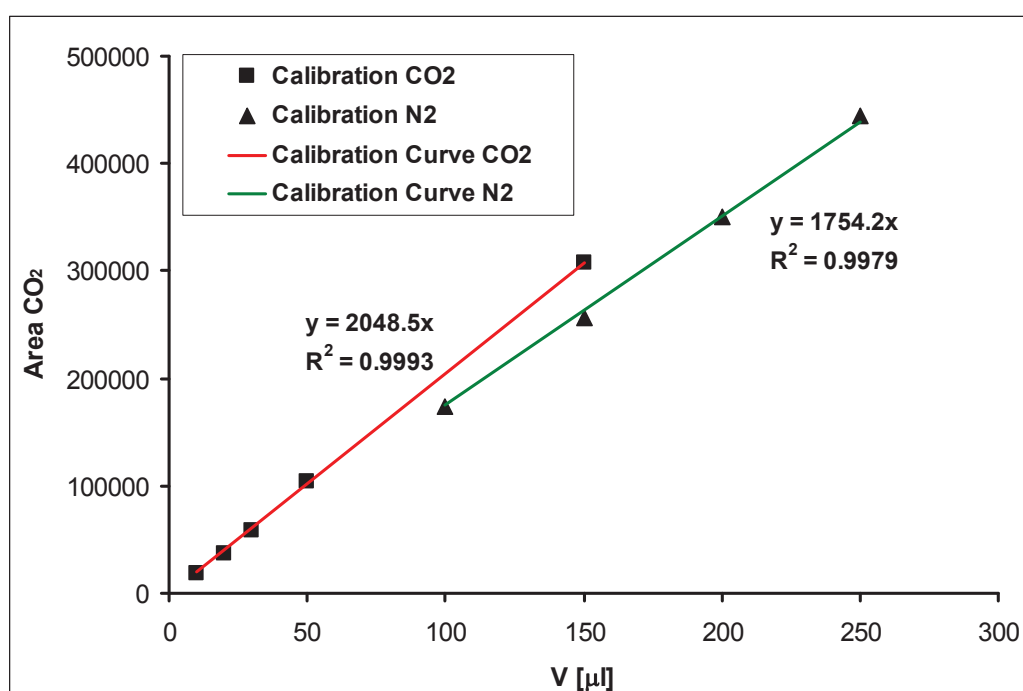


Figure 24: Calibration Curve for CO<sub>2</sub> and N<sub>2</sub> at GC settings of 240/120°C and 100mA.

With the area of the CO<sub>2</sub> and the N<sub>2</sub> peak obtained from the integration or software of the GC, it is possible to convert this area into a volume according the calibration curve.

## 3.3 Analyses of Sulphur in Liquid Solutions

For the SO<sub>2</sub> and CO<sub>2</sub> loaded potassium carbonate solutions, the determination of sulphur or sulphur species is essential to the investigation of the effect of SO<sub>2</sub> on the equilibrium partial pressure of CO<sub>2</sub>.

However, due to the presence of potassium carbonate, the determination of the sulphur is complicated. Normally the standard technique for the analysis of sulphur species is the precipitation as the sulphate species using Barium [28]. This method does not work because

of the interference with the carbonate ion. Another common method, is iodometric titration, this also does not work because of the high pH of the carbonate solution. Iodometric titration requires a slightly acid pH, however the pH of the potassium carbonate solution is greater than 12.

Two different analytical techniques were used to analyse the dissolved  $\text{SO}_2$ . The total amount of sulphur dissolved in the potassium carbonate solution was determined using ICP - AES (Inductively Coupled Plasma - Atomic Emission Spectrometer). For a qualitative and semi - quantitative analysis of the sulphur species formed FTIR (Fourier Transform Infrared Spectroscopy) was used.

### 3.3.1 Analysis with FTIR (Fourier Transform Infrared Spectroscopy)

FTIR (Fourier Transform Infrared Spectroscopy) was used as a qualitative and semi - quantitative determination for the formed species after the absorption of both  $\text{SO}_2$  and  $\text{CO}_2$ .

#### 3.3.1.1 Basics about Infrared (IR) and FTIR Spectroscopy

The principle behind infrared spectroscopy is that nearly all molecular species absorb infrared radiation and each has a unique or characteristic infrared absorption spectra. Unlike ICP - AES which is an elemental analysis based on individual atoms, FTIR is a molecule-specific method. That yields information about functional groups and bonding present within a molecule. The IR spectrum is obtained by measuring the intensity of the absorption of monochromatic radiation across a range of wavelengths passed through a sample. After passing through the sample, the monochromatic beam has a reduced intensity as a result of absorption in the sample. The loss of intensity at a certain wavelength is characteristic to each molecule.

Instead of a monochromator or dispersing elements to create the necessary beam, Fourier transform instruments use a Michelson interferometer for coding the polychromatic spectrum of the source. To separate the wavelengths, it is necessary to modulate the source signal that it can be decoded using Fourier transformation. The advantage of the FTIR is the very precise mechanism, the high sensitivity and resolution and the speed of the data acquisition.

#### 3.3.1.2 Samples Preparation and Background

A VARIAN 7000 FT-IR Spectrometer was used for all the IR measurements. All the samples were analysed as a liquid drop on the ATR cell. For higher loadings where precipitation occurred at room temperature, the samples were reheated such that all the species were in solution at the time of analysis. Different background spectra were tested, however, for the qualitative and semi - quantitative analysis a pure  $\text{K}_2\text{CO}_3$  solution gave the best result. This background was the spectrum of a pure, unloaded potassium carbonate solution that was subtracted from the spectra obtained for the  $\text{SO}_2$  and  $\text{CO}_2$  loaded solutions. The resulting spectrum shows directly the change in species due to the absorption of  $\text{CO}_2$  and  $\text{SO}_2$ . The



observed peaks were then compared with spectra from literature and the likely species present were identified.

For the quantitative analysis of sulphite ( $\text{SO}_3^{2-}$ ), a calibration curve for sulphite was made. Standards were prepared by dissolving different amounts of sodium – sulphite ( $\text{Na}_2\text{SO}_3$ ) in potassium carbonate solution and then analysed by FTIR. The heights of the  $\text{SO}_3^{2-}$  peaks were directly proportional to the corresponding amount of dissolved sulphite result and hence could be used as the calibration curve for quantitative analyses. This was used to quantify the sulphite species present in the samples.

### 3.3.2 Analysis with ICP - AES (Inductively Coupled Plasma - Atomic Emission Spectrometer)

Inductively coupled plasma spectroscopy (ICP) is an atomic spectroscopy method that uses a plasma for the atomization of the sample.

#### 3.3.2.1 Basic about Atomic Spectroscopy

“Atomization is a process in which a sample is converted into gaseous atoms or elementary ions.” [20, p. 611]

Atomization of a sample causes the atoms to absorb energy, which in turn promotes the single outer - shell electrons to rise from their ground state to an excited state orbital. After a short time period, a microsecond or less, the atoms fall back to their original ground state by releasing the absorbed energy as photons of visible or ultraviolet radiation. The wavelength of the emitted radiation is characteristic to each detectable element, with the intensity of the emitted radiation proportional to the concentration of the element. The most widely used atomic spectroscopy technique is based upon flame atomization, where the atomization takes place in a flame at temperatures of 1700 – 3200°C.

#### 3.3.2.2 Basics about ICP - AES

As mentioned earlier, in an ICP the atomization takes place in a plasma.

“A plasma is a conducting gaseous mixture containing a significant concentration of cations and electrons. “ [20, pp. 632]

The main advantages of ICP as the method for atomization are the high temperature and energy available from the plasma and hence the detection limits can be really low, in the range of parts per billion (ng/l) to parts per million (mg/l). The typical ICP plasma is very intense, brilliant white and optical thin, which results in less interference with the emission spectrum of the sample. For the emission analysis, argon plasma, with a temperature range from 6000 – 8000K, is generally used. The residence time for the atoms in the plasma is about 2ms. Compared with the flame atomic spectroscopy, the plasma temperature is about



two to three times hotter than the hottest combustion flames. As a consequence, the atomization of the sample is more complete, with the benefit of less chemical interference. The analysis of the solution is achieved by the introduction of the samples into the plasma as an aerosol.

### 3.3.2.3 Sample and Standard Preparation

Due to the detection limits of ICP and to reduced matrix background effects from the potassium carbonate solution, the samples were diluted with deionised water. For the first series of samples the sulphur concentrations were not known, hence different dilution factors were tested to get knowledge of the concentrations of the sulphur absorbed by the potassium carbonate solution. For the subsequent samples, the approximate concentration range of sulphur for the three different loaded solutions was known. The dilution factor was chosen such that the concentration of the sulphur was approximately 100ppm (mg/l).

Depending on the solution sulphur loadings, the dilution factors were 167x for the highest concentration of absorbed  $\text{SO}_2$ , 100x for the middle concentration and 67x for the lowest concentration. For each sample one litre of the diluted solution was prepared. This required the use of 6ml, 10ml or 15ml of loaded  $\text{K}_2\text{CO}_3$  solution/litre of the three different sulphur concentrations. To increase the accuracy of the sulphur determination 5 samples with different  $\text{CO}_2$  loadings were analysed for each sulphur concentration.

Standard solutions were prepared with total sulphur concentrations of 50ppm, 100ppm and 200ppm from potassium sulphate ( $\text{K}_2\text{SO}_4$ ) which was dissolved in deionised water. For the calibration curve these three standards and a blank were used with the emission intensity measured at four different wavelengths characteristic to sulphur. The use of the multiple wavelengths is recommended, as spectral interferences may occur if the characteristic wavelength of one element coincides with that of another.

All ICP analysis of the standards and samples were performed on a Varian 720 - ES by a trained operator.

## 4 Results / Discussion

### 4.1 The CO<sub>2</sub> Equilibrium Curve

The CO<sub>2</sub> equilibrium curve over a potassium carbonate solution has been studied in detail by Tosh et al., with the results published in the paper “Equilibrium study of the system potassium carbonate, potassium bicarbonate, carbon dioxide and water” [12]. The paper presents the equilibrium partial pressure of carbon dioxide and water vapour over a 20w%, 30w% and 40w% potassium carbonate solution, for the temperature range from 70 – 130°C.

To verify the operation and validity of the vapour – liquid equilibrium rig, shown in Figure 21, measurements for a CO<sub>2</sub> loaded 30w% potassium carbonate solution were made and compared with that reported in literature. From this comparison it was possible to determine whether vapour – liquid equilibrium could be achieved and that subsequent measurements for the SO<sub>2</sub> – CO<sub>2</sub> – K<sub>2</sub>CO<sub>3</sub> system would yield meaningful results.

#### 4.1.1 Calculation of the CO<sub>2</sub> Equilibrium Partial Pressure from the Experimental Results

Vapour – liquid equilibrium measurements were taken at temperatures of 90°C and 100°C. At each temperature four points were obtained by using solutions with differing CO<sub>2</sub> loadings between 0.1 and 0.35. The CO<sub>2</sub> loading of the solution is equal to the degree of saturation as defined in Section 2.1.2.1.1 and is calculated using Equation(63):

$$y_{\text{loading}} = \frac{[\text{HCO}_3^-]}{2 \cdot [\text{CO}_3^{2-}] + [\text{HCO}_3^-]} \quad (63)$$

The solution CO<sub>2</sub> loading was measured before and after each equilibrium test. In all cases the CO<sub>2</sub> loading of the solution was observed to decrease slightly, which was to be expected as some of the CO<sub>2</sub> in the solution transfers to the gaseous phase. After reaching the equilibrium point (runtime approximately 2 hours after thermal equilibrium), the gas and liquid samples were taken. For the gas sample the GC injection volume was 250 μl, while a 2ml liquid sample was analysed by titration. The result of the titration showed directly the carbonate and bicarbonate concentrations, hence the CO<sub>2</sub> loading of the solution could be calculated using Equation(63). For the liquid analysis three samples were taken from the second vessel. However, due to the larger variation observed for gas analysis, at least five samples were taken. In instance that the variation of the measured peak areas was deemed too large, more samples were taken until a consistent reading was achieved.

According to the GC calibration curve, the obtained peak areas are proportional to the volume fraction. For an ideal gas, which can be assumed for these experiments because the pressure was atmospheric and the temperature of the cooled gas stream was approximately room temperature, the volume fraction is equivalent to the molar fraction.



$$y_i = \frac{Ar_i}{k_i \cdot V_{\text{Syringe}}} \cdot 100 \quad (64)$$

- $y_i$  = mole fraction of component i in gas phase [mol<sub>i</sub>/mol<sub>ges</sub>]  
 $Ar_i$  = area of component i obtained from GC  
 $k_i$  = slope of the calibration curve for component i [1/μl]  
 $V_{\text{Syringe}}$  = injected volume into the GC [μl]

Due to the fact that only nitrogen and carbon dioxide were present in the gas samples (the water vapour can be neglected at this low temperature), the sum of the molar or volumetric fraction has to be 1. As a result of the experimental uncertainty in the calibration curve and variation in the injected volume of the gas samples, the calculated molar fractions were normalized to 1. In most cases the deviation from 100% was less than 4 to 5%.

$$y_{i,\text{norm}} = \frac{y_i}{\sum y_i} \quad (65)$$

- $y_{i,\text{norm}}$  = normalized mole fraction of component i in gas phase [mol<sub>i</sub>/mol<sub>ges</sub>]

From the obtained molar fraction of carbon dioxide in the gas phase, the equilibrium partial pressure can be calculated using Dalton's Law.

$$p^*_{\text{CO}_2} = y_{\text{CO}_2} \cdot p_{\text{tot}} \quad (66)$$

The errors of the calculation and measurement were calculated with a 95% confidence interval. The absolute and the relative error were calculated for the standard deviation of the measured peak area [20].

$$f_a = \frac{1.96 \cdot \sigma(Ar_i)}{k_i \cdot V_{\text{Syringe}}} \cdot 100 \quad (67)$$

$$f_r = \frac{f_a}{p^*_{\text{CO}_2}} \cdot 100 \quad (68)$$

- $\sigma(Ar_i)$  = standard deviation of the measured area  
 $f_a$  = absolute error of the equilibrium partial pressure [kPa]  
 $f_r$  = relative error of the equilibrium partial pressure [%]

The calculated and measured partial pressures of CO<sub>2</sub> were those over the potassium carbonate solution with a water vapour pressure at approximately 25°C (room temperature). As shown in Figure 21, the gas samples were taken after the gas had been cooled to the ambient temperature by the condenser. The reason for cooling was to drop out the majority



of the water from the gas because the GC was not setup to analyse for water and hence display it as a quantifiable peak. At 25°C the water vapour pressure is really low in comparison to 90°C or 100°C. It was found that nearly no water was dropped out in the condenser at experimental temperatures of 90°C and 100°C. Due to the low gas flow rate, the gas already had been cooled down to ambient temperature in the pipe after the second vessel and so the water condensed back into the vessel.

For a direct comparison of the obtained experimental results with those reported in the literature, an ASPEN PLUS simulation for the CO<sub>2</sub> – K<sub>2</sub>CO<sub>3</sub> system was used. The simulation calculated both, the equilibrium partial pressure of carbon dioxide at 90 and 100°C with a water vapour pressure of 25°C and the actual equilibrium partial pressure including the water vapour pressure at 90 and 100°C. The difference between the simulation at a water vapour pressure of 25°C and that for a dry nitrogen and carbon dioxide gas is relatively small due to the low water vapour pressure at 25°C. The fact that the experimental results fit closely to the simulation with a water vapour pressure at 25°C, validates the operating mode of the experimental rig. To determine the actual equilibrium pressure over a 30w% potassium carbonate solution at 90 and 100°C, with the inclusion of water vapour at these temperatures, a correction factor was introduced. The correction factor was calculated from the relationship between the simulated ASPEN PLUS results with water vapour at 25°C and 90 or 100°C.

$$\frac{p_{\text{CO}_2, \text{H}_2\text{O}/T}^*}{p_{\text{CO}_2, \text{H}_2\text{O}/25\text{C}}^*} = \frac{f(p_{\text{ASPEN}/T}^*)}{f(p_{\text{ASPEN}/25\text{C}}^*)} \quad (69)$$

$p_{\text{CO}_2, \text{H}_2\text{O}/T}^*$	=	equilibrium partial pressure of CO <sub>2</sub> at temperature T (90 or 100°C) [kPa]
$p_{\text{CO}_2, \text{H}_2\text{O}/25\text{C}}^*$	=	partial pressure of CO <sub>2</sub> with a water vapour pressure at 25°C (experimental result) [kPa]
$f(p_{\text{ASPEN}/T}^*)$	=	equation of equilibrium curve at temperature T (90 or 100°C)
$f(p_{\text{ASPEN}/25\text{C}}^*)$	=	equation of equilibrium curve with a water vapour pressure at 25°C

The correction factor was then calculated from a 3<sup>rd</sup> order polynomial fit that was made for the equilibrium curves at each temperature. The correction factor is then calculated through dividing the polynomial fits according to Equation(69). The factor is partially depended on the CO<sub>2</sub> loading of the solution and hence was calculated for each experimental point. The dependency on the loading was however relatively low as the correction factor was observed to be nearly constant for each temperature. At 90°C the correction factor was approximately 0.5, while at 100°C the factor was around 0.3.

As observed in the calculation of the correction factor for the different CO<sub>2</sub> loadings, the factor and the water vapour pressure did not change significantly with changes in the CO<sub>2</sub> loading. Tosh et al. [12] also reported that the water vapour pressure over a 30w% potassium carbonate solution was almost constant over a range of different CO<sub>2</sub> loadings. This would suggest that the calculation of the equilibrium partial pressure from the obtained



experimental data using this correction factor was valid. Furthermore, the fact that the experimental data points fit closely with the ASPEN PLUS simulation including the water vapour pressure at 25°C, implies that the experimental points would also agree with the equilibrium curve incorporating the water vapour pressure at 90 and 100°C.

The correction factor was also used to calculate the equilibrium partial pressure for the  $\text{SO}_2 - \text{CO}_2 - \text{K}_2\text{CO}_3$  system at 90 and 100°C.

#### 4.1.2 Equilibrium Curves for the System $\text{CO}_2 - \text{K}_2\text{CO}_3$

The equilibrium curve results for the  $\text{CO}_2 - \text{K}_2\text{CO}_3$  vapour - liquid experiments and simulations, with a water vapour pressure at 25°C for both temperatures 90 and 100°C, are presented in Figure 25. These curves were then transformed to the vapour – liquid equilibrium curves over a 30w% potassium carbonate solution, as shown in Figure 26 and Figure 27, by using the correction factor described earlier. A comparison to the data reported in the literature by Tosh et al. [12] and Savage et al. [11] is given for each curve.

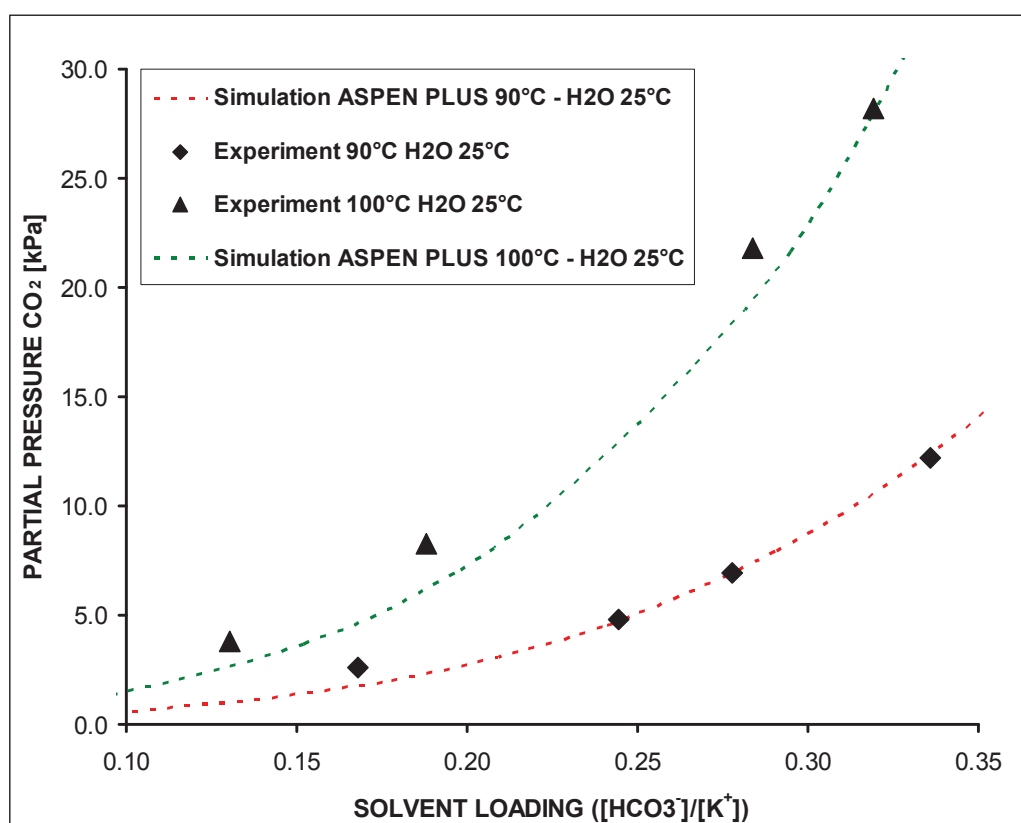
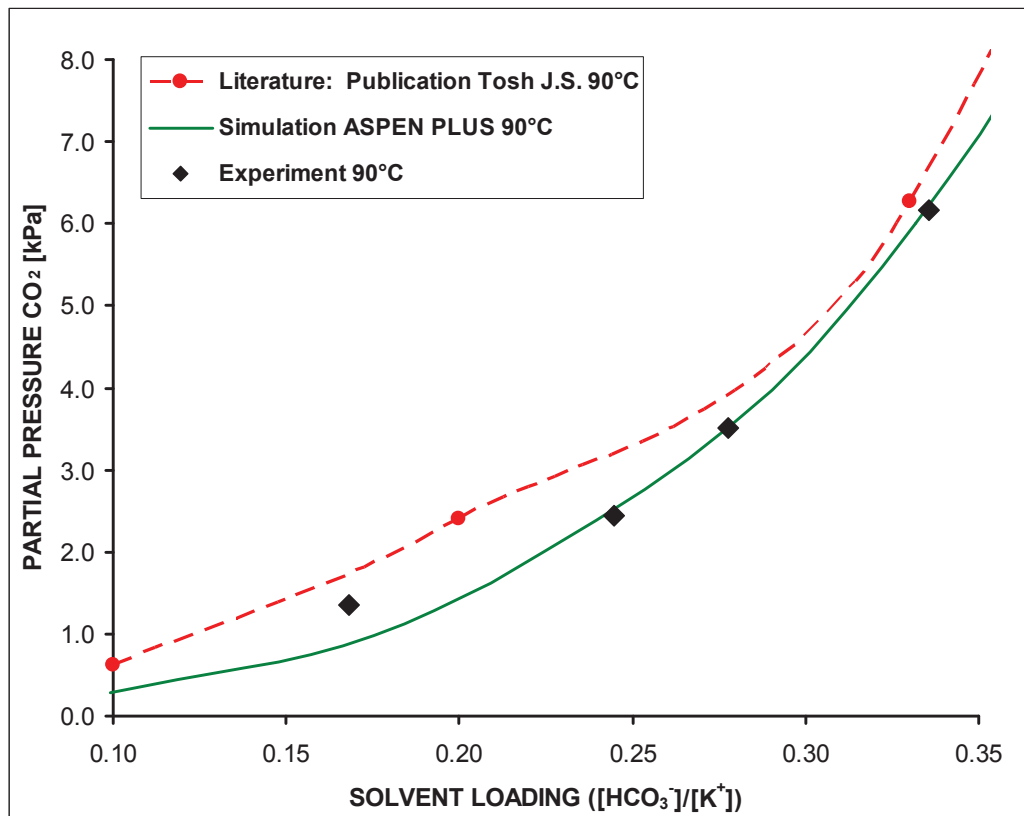
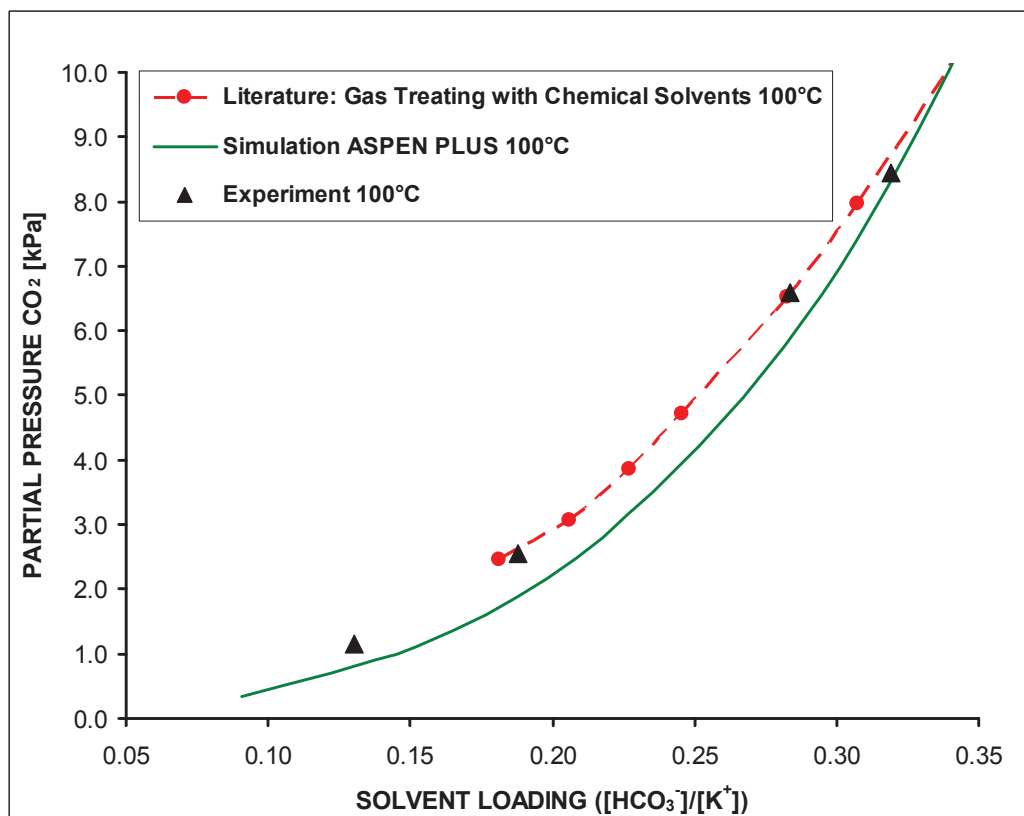


Figure 25: Equilibrium curve of  $\text{CO}_2$  over 30w% potassium carbonate solution at a water vapour pressure of 25°C.

Figure 26: Equilibrium curve of CO<sub>2</sub> over 30w% potassium carbonate solution at 90°C.Figure 27: Equilibrium curve of CO<sub>2</sub> over 30w% potassium carbonate solution at 100°C.

The values of the obtained results from the vapour – liquid experiment with a water vapour pressure at 25°C and the actual equilibrium pressure for 90°C and 100°C are summarized in Table 3.

Table 3: Experimental equilibrium data points of CO<sub>2</sub> over 30w% potassium carbonate solution at 90 and 100°C.

<i>Loading</i>	<i>Partial Pressure of CO<sub>2</sub> with water vapour at 25°C</i> [kPa]	<i>Equilibrium Partial Pressure of CO<sub>2</sub> including the water vapour pressure</i> [kPa]
<b>90°C</b>		
0.17	2.60	1.36
0.24	4.77	2.44
0.28	6.92	3.51
0.34	12.23	6.16
0.43	22.95	11.50
<b>100°C</b>		
0.13	3.79	1.16
0.19	8.29	2.54
0.28	21.83	6.58
0.32	28.21	8.45
0.39	41.20	12.21

As shown in Table 3, two measurements contain a CO<sub>2</sub> loading of approximately 0.4. At such high CO<sub>2</sub> loadings, the experimental result did not fit with that reported in the literature or the simulation result. The main reason for this could be that the VL equilibrium rig used only had two vessels, however the design on which the rig was based had three vessels in series [9],[10]. Hence it is possible that the VL equilibrium is not achieved at such high solution CO<sub>2</sub> loadings. For this reason, these points were excluded from the diagrams in Figure 26 and Figure 27.

## 4.2 Solvent Concentration of Sulphur

As described earlier in Section 3.3.2, the concentration of absorbed SO<sub>2</sub> in the K<sub>2</sub>CO<sub>3</sub> solution was determined by total sulphur analysis, which was performed by ICP.

For each of the three different sulphur concentrations, 5 samples with different CO<sub>2</sub> loadings were analysed. However, for the 1/8 dilution and the 1/16 dilution one value was neglected, as these results were considered erroneous.

The results from the ICP analysis were the concentrations of sulphur for the diluted samples. The results were in ppm, which is equivalent to mg/l as the major component of the samples was deionised water as a result of the dilution. As the deionised water did not contain any sulphur, the measured amount of sulphur in the diluted solution, was equal to the amount of

sulphur in the undiluted  $K_2CO_3$  solution samples. The sulphur concentrations in the undiluted  $K_2CO_3$  solution samples are given by Equation(70).

$$X_{Sulphur} = \frac{X_{Sulphur,diluted}}{V_{K_2CO_3}} \quad (70)$$

$X_{Sulphur}$  = concentration of sulphur in the loaded  $K_2CO_3$  solution [g/l]  
 $X_{Sulphur,diluted}$  = concentration of sulphur in diluted solution (result from ICP) [mg/l]  
 $V_{K_2CO_3}$  = volume of loaded  $K_2CO_3$  solution added for dilution [ml/l]

The results obtained from the ICP analysis and the calculated concentrations of sulphur in  $CO_2$  and  $SO_2$  loaded solutions in  $g_{Sulphur}/l_{K_2CO_3Solution}$  and  $mol_{Sulphur}/l_{K_2CO_3Solution}$  are presented in Table 4.

Table 4: Total sulphur concentration of the loaded  $K_2CO_3$  solutions.

		1/8 Dilution			1/16 Dilution			1/25 Dilution		
Measured Concentration of diluted samples from ICP	[mg/l]	115.2 113.5	114.2	116.2	103.7 107.0	100.5	103.0	98.9 107.8	96.8 106.0	96.9
Average Concentration of diluted samples from ICP	[mg/l]	114.7			103.5			101.3		
Dilution factor:		1/167			1/100			1/67		
Volume of $K_2CO_3$ / l	[ml/l]	6.00			10.00			15.00		
Average sulphur concentration of $K_2CO_3$ solution	[g/l]	<b>19.12</b>			<b>10.35</b>			<b>6.75</b>		
Average sulphur concentration of $K_2CO_3$ solution	[mol/l]	<b>0.60</b>			<b>0.32</b>			<b>0.21</b>		

The samples with  $CO_2$  loadings used for the ICP analysis, were taken at the completion of the VL equilibrium test run, which means that the solution had been maintained at a temperature within the range of 90 -100°C for at least several hours. Compared to the first sample without absorbed  $CO_2$ , which was not used for the VL experiment, the concentration of the total sulphur remained constant. This would suggest that the absorption of the  $SO_2$  was a non – reversible reaction for this temperature range. As a consequence, the  $SO_2$  would most likely not be stripped out during solvent regeneration in the stripping column, as will be discussed further in Section 4.5.1.

## 4.3 Sulphur Speciation

### 4.3.1 Qualitative Analysis of the Formed Species

An FTIR spectrum of a sample solution that was used for qualitative analysis of the formed species after the absorption of  $SO_2$  and  $CO_2$ , is presented in Figure 28.

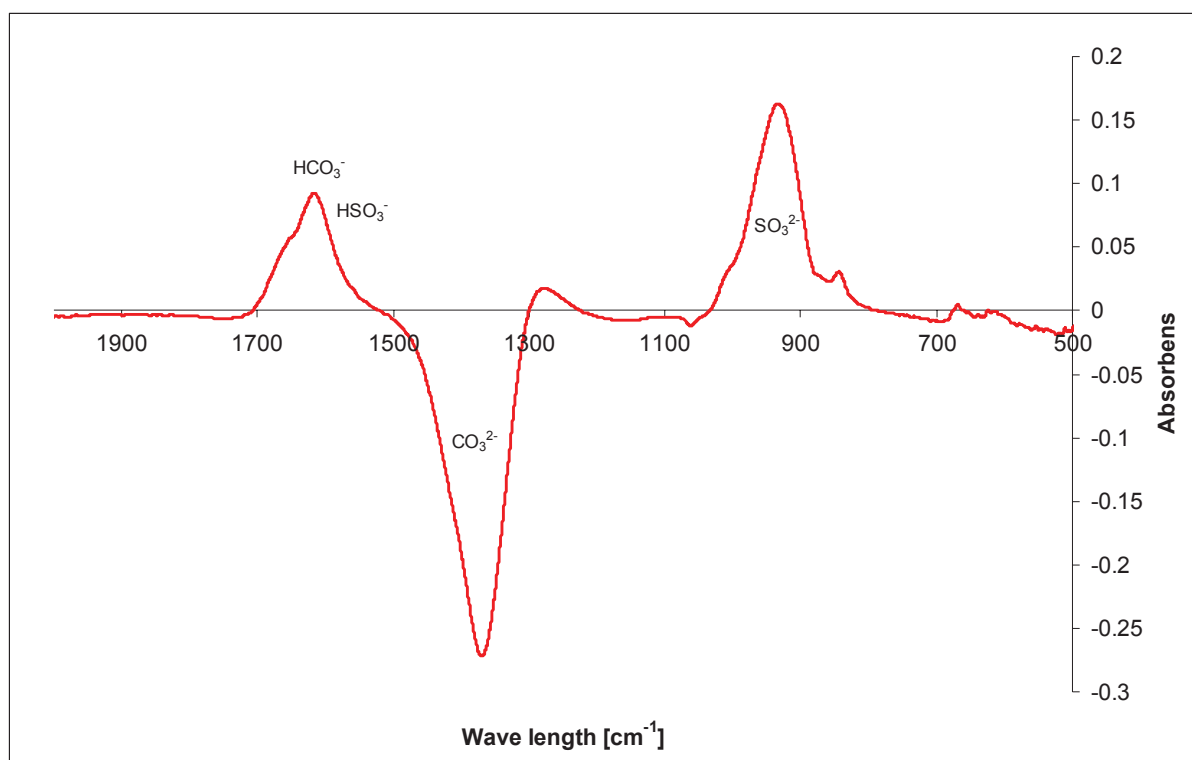


Figure 28: FTIR spectrum of a CO<sub>2</sub> and SO<sub>2</sub> loaded solution.

As a K<sub>2</sub>CO<sub>3</sub> background was used the formed species could be easily identified, with three major peaks observed in the FTIR spectra as seen on Figure 28. At wave length between 850 and 1050 cm<sup>-1</sup> the sulphite (SO<sub>3</sub><sup>2-</sup>) peak is observed. The presence of sulphite agrees with the SO<sub>2</sub> absorption reaction suggested earlier, Equation(54), with the wave length range of the peak is comparable to the spectrum reported in the literature for sulphite [31].

The negative peak in the 1300 to 1500 cm<sup>-1</sup> wavelength range was that for carbonate species (CO<sub>3</sub><sup>2-</sup>). The decrease of the carbonate concentration was due to the absorption of CO<sub>2</sub> (Equation(44)) and the release and capture of CO<sub>2</sub> during the absorption of SO<sub>2</sub> (Equation (54) and (55)). Both reactions convert carbonate (K<sub>2</sub>CO<sub>3</sub>) to bicarbonate (HCO<sub>3</sub><sup>-</sup>) due to the reaction with CO<sub>2</sub>. The formed bicarbonate species was observed on the FTIR spectrum as a peak at wavelength between 1500 and 1700 cm<sup>-1</sup>. It was possible that this peak overlaps with that of bisulphite (HSO<sub>3</sub><sup>-</sup>) species, hence a qualitative separation was not possible. Each of the three observed peaks fit the expected reactions for the absorption of CO<sub>2</sub> and SO<sub>2</sub> and the spectra for these species reported in the literature [32].

Other sulphur species like sulphate (SO<sub>4</sub><sup>2-</sup>) and bisulphate (HSO<sub>4</sub><sup>-</sup>), which could also be expected to form from side reactions (Equation(57)), were not observed to form. According to the literature, the peak for sulphate should be observed at wave length of approximately 1150 cm<sup>-1</sup> and for bisulphate at 1200 cm<sup>-1</sup> [32]. It was evident from the spectra obtained that there clearly was no peak, which would imply that neither species was formed. This result also agrees with the solubility of sulphate in a potassium carbonate solution which is

discussed further in Section 4.5.2, which indicates that sulphate is virtually insoluble in potassium carbonate solutions.

### 4.3.2 Determination of the Sulphite ( $\text{SO}_3^{2-}$ ) Concentration

Samples with different sulphur and  $\text{CO}_2$  concentrations were analysed using FTIR. It would be expected that the sulphite concentration and hence the height of the measured  $\text{SO}_3^{2-}$  peak would be independent of the  $\text{CO}_2$  loading. However, as the FTIR analysis could not be completed immediately after sampling, the solution samples were allowed to cool and were kept for longer periods of time. The potassium carbonate solution was a colourless transparent solution but some samples taken at the completion of the equilibrium experiments were slightly turbid, due to contamination prior to analysis by FTIR. As the experiments were performed in an oil bath, it was likely that during the opening of the vessel and solution sampling, some oil contamination of the samples occurred. For the higher sulphur concentrated solution (1/8 and 1/16 dilution), precipitation of sulphate was observed after extended periods. The likely reason for this was that all the samples were stored in sample containers which had a head space volume of air and hence oxygen for Reaction(57) was present and enabled the formation of sulphate. This precipitation inherently effects the concentration of the sulphite species.

As shown in Table 5, it was possible to obtain reasonable quantification of the sulphite concentration for each of the three different sulphur loadings by FTIR analysis. The results clearly imply that the absorbed  $\text{SO}_2$  formed the sulphite species as the measured sulphite concentration was observed to have an equivalent sulphur concentration to the total sulphur concentration obtained by ICP analysis. This would indicate that the main reaction that occurs during the absorption of  $\text{SO}_2$  in the potassium carbonate solution, was the formation of sulphite, Reaction(54). The formation of bisulphite was only a side reaction due to the insignificant concentration of bisulphite observed.

Table 5: Sulphite ( $\text{SO}_3^{2-}$ ) concentration of the loaded  $\text{K}_2\text{CO}_3$  solutions.

		Total Sulphur 19.12 g/l	Total Sulphur 10.35 g/l	Total Sulphur 6.75 g/l
Total sulphur concentration obtained from ICP analysis	[mol/l]	0.60	0.32	0.21
Average sulphite ( $\text{SO}_3^{2-}$ ) concentration	[mol/l]	0.60	0.32	0.19
Average sulphite ( $\text{SO}_3^{2-}$ ) concentration	[g/l]	48.16	25.44	14.86

## 4.4 The Effect of SO<sub>2</sub> on the Equilibrium Curve of CO<sub>2</sub>

The equilibrium curve for the partial pressure of CO<sub>2</sub> with three different sulphur concentrations in the K<sub>2</sub>CO<sub>3</sub> solution was studied. For each concentration at least four vapour – liquid equilibrium points at the temperatures of 90 and 100°C were measured. The experimental methods and the sample analysis were essentially the same as described in Section 4.1.1, however some slight modifications as described as followed were used to allow direct comparison with the results of the base CO<sub>2</sub> – K<sub>2</sub>CO<sub>3</sub> system.

The fact that during the absorption of SO<sub>2</sub>, as described by Equation(54), CO<sub>2</sub> is released by the carbonate and then reabsorbed to form bicarbonate, results in a pre-loading of CO<sub>2</sub> in the solution. This affects the value of the solvent loading, which is the value of the x-axes of the equilibrium curve. The solution CO<sub>2</sub> loading can either be expressed as the total loading including the pre-loading due to the SO<sub>2</sub> and the actual absorbed CO<sub>2</sub>, or only the actual loading of the absorbed CO<sub>2</sub>. The actual loading of absorbed CO<sub>2</sub> ( $y_{loading,CO_2}$ ) was the difference of the total loading ( $y_{loading,total}$ ) at the completion of the equilibrium test and the pre-loading resulting from the SO<sub>2</sub> loaded solution ( $y_{loading,SO_2}$ ).

$$y_{loading,CO_2} = y_{loading,total} - y_{loading,SO_2} \quad (71)$$

For the study of the absorption efficiency and the influence of SO<sub>2</sub> on the CO<sub>2</sub> equilibrium partial pressure, the actual CO<sub>2</sub> loading of the solvent was of greater significance. This loading value shows directly the effect of SO<sub>2</sub> on the CO<sub>2</sub> equilibrium that is, it demonstrates the free capacity for the absorption of CO<sub>2</sub>.

The molar fractions  $y_i$  for nitrogen and carbon dioxide calculated from the GC analysis were not normalized as was done for the CO<sub>2</sub> – K<sub>2</sub>CO<sub>3</sub> system. This was due to the fact that it could not be excluded that there may have been some other species present in the gas stream that was not detected by the GC. The fractions were normalised only when the total molar fraction was more than 1.

To include the partial pressure of water, the same correction was made as for the CO<sub>2</sub> – K<sub>2</sub>CO<sub>3</sub> system, discussed earlier. It was assumed that the partial pressure of water over the potassium solution was the same for both systems and was only depending on the temperature.

### 4.4.1 Equilibrium Curves for the System SO<sub>2</sub> - CO<sub>2</sub> – K<sub>2</sub>CO<sub>3</sub>

Both Figure 29 and Figure 30 show the effect of absorbed SO<sub>2</sub> on the equilibrium partial pressure curve of CO<sub>2</sub>. As shown the experimental data points were fitted with a best fit trend line of the form  $y=a*x^b$ .



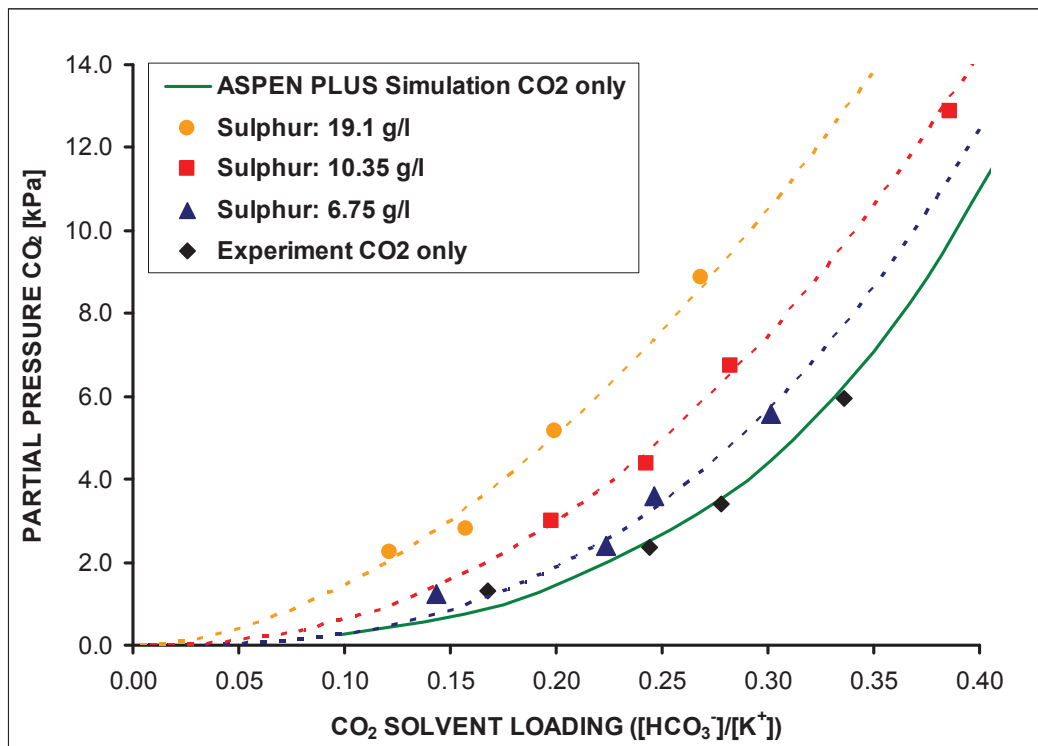


Figure 29: Equilibrium curve of CO<sub>2</sub> over 30w% potassium carbonate solution at 90°C for different sulphur concentrations.

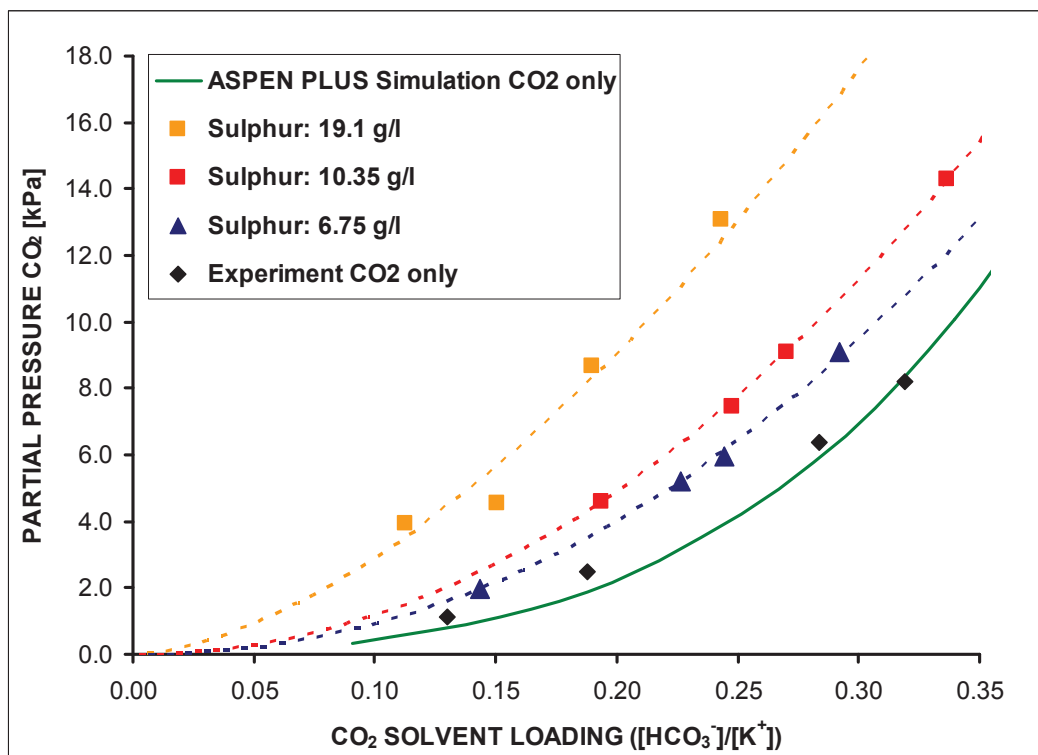


Figure 30: Equilibrium curve of CO<sub>2</sub> over 30w% potassium carbonate solution at 100°C for different sulphur concentrations.

It was evident that the absorption of sulphur dioxide by the potassium carbonate solutions resulted in a shift of the CO<sub>2</sub> equilibrium curve to the left. With increasing sulphur concentration, the curve was observed to shift more to the left. This would imply that the ability of the potassium carbonate solution to absorb CO<sub>2</sub> from the gas stream decreases with an increase in the absorbed SO<sub>2</sub>. This result would be reasonable and can be explained by using Equation (54) and Equation(55). During the absorption of SO<sub>2</sub> and the formation of potassium sulphite, carbon dioxide is formed and released. The released CO<sub>2</sub> is then directly absorbed by the fresh carbonate solution to form bicarbonate which would be equivalent to a pre-loading with additional CO<sub>2</sub>. Furthermore, it means that the potassium carbonate solution would have effectively a lower capacity to absorb CO<sub>2</sub> from the gas stream. In effect, it results in a higher observed equilibrium partial pressure for a certain loading or conversely in a lower loading for a certain partial pressure.

Summarized in Table 6 and Table 7 are the vapour – liquid equilibrium results obtained from the experiments with a water vapour pressure at 25°C and the actual equilibrium partial pressure of CO<sub>2</sub> for 90°C and 100°C calculated over the correction factor. Also given on each table are the values of the total SO<sub>2</sub> and CO<sub>2</sub> loading, the actual CO<sub>2</sub> loading and the loading for the transpose points presented in Figure 31 and Figure 32.

Table 6: Experimental results of the SO<sub>2</sub> and CO<sub>2</sub> equilibrium curve at 90°C.

Experimental Results of the SO <sub>2</sub> and CO <sub>2</sub> equilibrium curve at 90°C					
Loading			Partial pressure of CO <sub>2</sub> with water vapour at 25°C [kPa]	Equilibrium partial pressure of CO <sub>2</sub> including the water vapour pressure [kPa]	
Total SO <sub>2</sub> and CO <sub>2</sub>	Only CO <sub>2</sub>	Shifted			
<b>Sulphur concentration 19.1 g/l</b>					
0.32	0.12	0.23	4.24	2.26	
0.35	0.16	0.26	5.30	2.79	
0.40	0.20	0.31	9.99	5.17	
0.47	0.27	0.38	17.46	8.87	
<b>Sulphur concentration 10.35 g/l</b>					
0.30	0.20	0.26	5.80	3.00	
0.34	0.24	0.30	8.58	4.38	
0.38	0.28	0.34	13.26	6.72	
0.48	0.39	0.45	25.69	12.90	
<b>Sulphur concentration 6.75 g/l</b>					
0.20	0.14	0.17	2.36	1.25	
0.28	0.22	0.25	4.67	2.40	
0.30	0.25	0.27	7.05	3.60	
0.35	0.30	0.32	11.03	5.58	

Table 7: Experimental results of the SO<sub>2</sub> and CO<sub>2</sub> equilibrium curve at 100°C.

Experimental Results of the SO <sub>2</sub> and CO <sub>2</sub> equilibrium curve at 100°C				
Loading			Partial pressure of CO <sub>2</sub> with water vapour at 25°C [kPa]	Equilibrium partial pressure of CO <sub>2</sub> including the water vapour pressure [kPa]
Total SO <sub>2</sub> and CO <sub>2</sub>	Only CO <sub>2</sub>	Shifted		
<b>Sulphur concentration 19.1 g/l</b>				
0.31	0.11	0.24	13.01	3.93
0.35	0.15	0.27	14.88	4.57
0.39	0.19	0.31	28.33	8.69
0.44	0.24	0.37	42.95	13.06
<b>Sulphur concentration 10.35 g/l</b>				
0.29	0.19	0.25	15.03	4.61
0.35	0.25	0.31	24.56	7.46
0.37	0.27	0.33	30.07	9.09
0.43	0.34	0.39	47.82	14.29
<b>Sulphur concentration 6.75 g/l</b>				
0.20	0.14	0.18	6.48	1.99
0.28	0.23	0.27	17.11	5.22
0.30	0.24	0.28	19.55	5.94
0.34	0.29	0.33	30.13	9.07

Both Figure 31 and Figure 32 demonstrate that the absorption of SO<sub>2</sub> transposes the equilibrium curve of CO<sub>2</sub> to the left, without altering the curve profile. To achieve this, the experimental points were shifted to the right, until they superimposed the equilibrium curve for the CO<sub>2</sub> – K<sub>2</sub>CO<sub>3</sub> system that is the solution with no absorbed SO<sub>2</sub>. The equation or the type of the fit was not altered. In all cases, the points match closely the simulated CO<sub>2</sub> equilibrium curve from ASPEN PLUS and those obtained experimentally for the CO<sub>2</sub> – K<sub>2</sub>CO<sub>3</sub> system. Despite the fact that for each sulphur concentration only 4 experimental points were obtained, the curve fit of each equilibrium curve overlaid the simulation with minimum discrepancy. This implies as mentioned earlier that the form of the equilibrium curve is independent of the absorbed SO<sub>2</sub> concentration.

The result at 90°C with a sulphur concentration of 10.35 g/l and a CO<sub>2</sub> loading of 0.39 was excluded from the curve fit, for the reasons discussed in Section 4.1 that is at higher CO<sub>2</sub> loadings the equilibrium rig fails to achieve vapour – liquid equilibrium. The first point at 90°C and a sulphur concentration of 6.75 g/l was also excluded, due to the fact that the CO<sub>2</sub> loading was observed to be really low and hence the measured peak areas for the GC gas analysis were really small and consequently the error was significant.

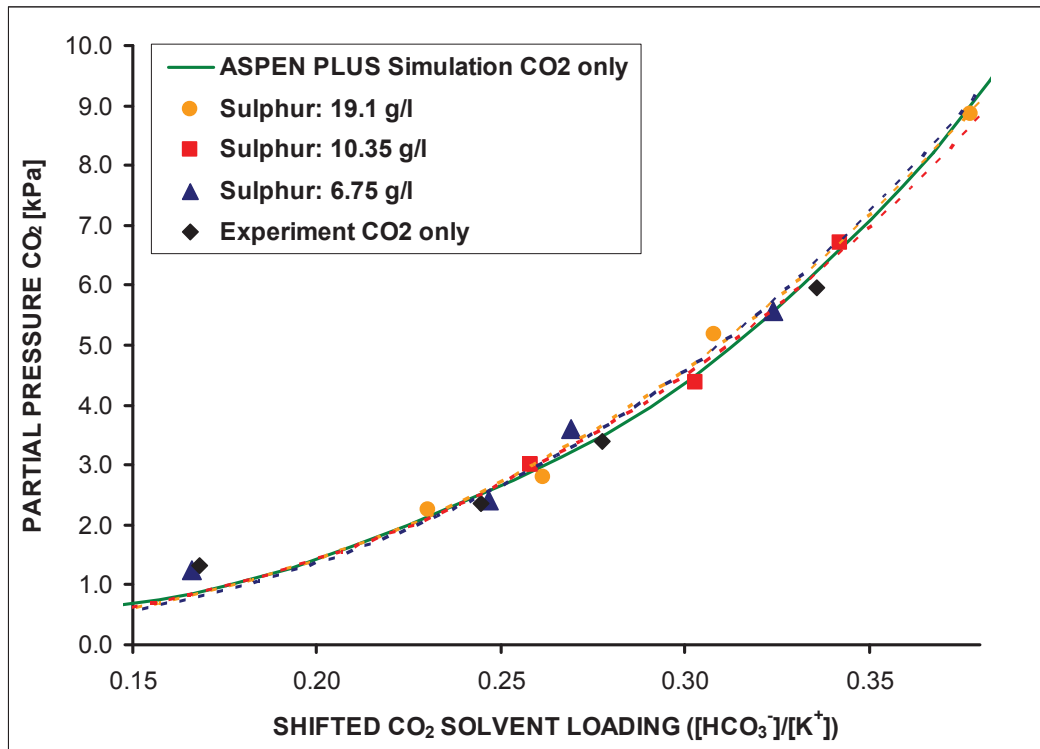


Figure 31: Shifted equilibrium curves of the different sulphur concentrations at 90°C.

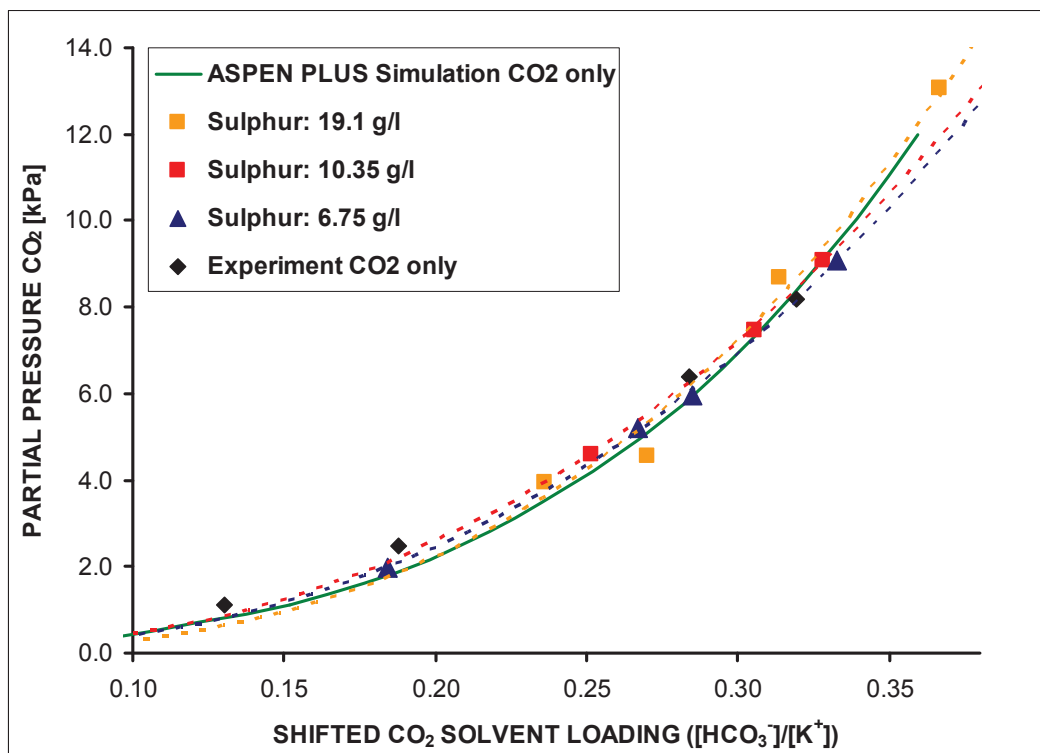


Figure 32: Shifted equilibrium curves of the different sulphur concentrations at 100°C.

#### 4.4.2 The Effect of Solvent Sulphur Concentration on the CO<sub>2</sub> Equilibrium Partial Pressure

Using the curve fitted equilibrium curves obtained from the experimental data points for the three different solution sulphur concentrations, it was possible to demonstrate the relationship between the dissolved SO<sub>2</sub> and the equilibrium partial pressure of CO<sub>2</sub>. As described earlier, the equilibrium partial pressure increased with an increase in the absorbed SO<sub>2</sub>. Figure 33 and Figure 34 show that the increase in equilibrium partial pressure, depended on the solvent sulphur concentration. For selected CO<sub>2</sub> loadings ( $y_{\text{loading}} = 0.15 - 0.35$ ), the equilibrium partial pressure of CO<sub>2</sub> for each of the three sulphur concentrations was calculated using the curve fit equation. These diagrams only represent qualitative a trend as the trend lines were based only on three different sulphur concentrations, hence the uncertainty or error could be significant. For a more accurate and reliable result, more measurements at different sulphur concentrations and more CO<sub>2</sub> loadings for each concentration should be completed.

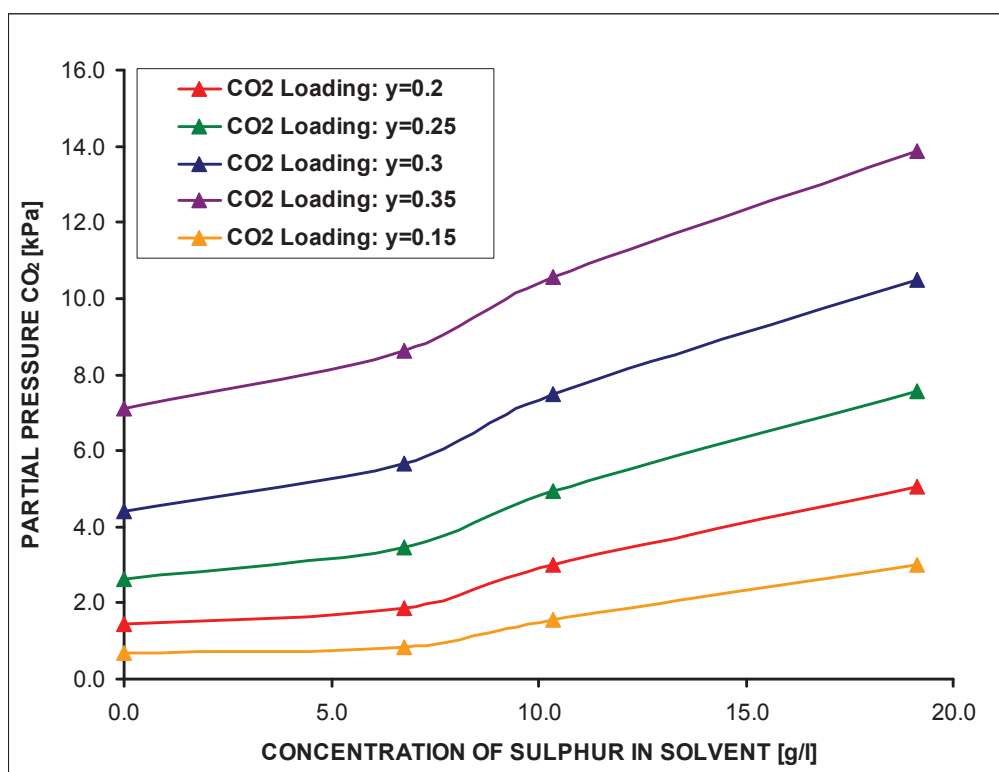


Figure 33: Effect of solvent sulphur concentration on the CO<sub>2</sub> equilibrium partial pressure at 90°C.

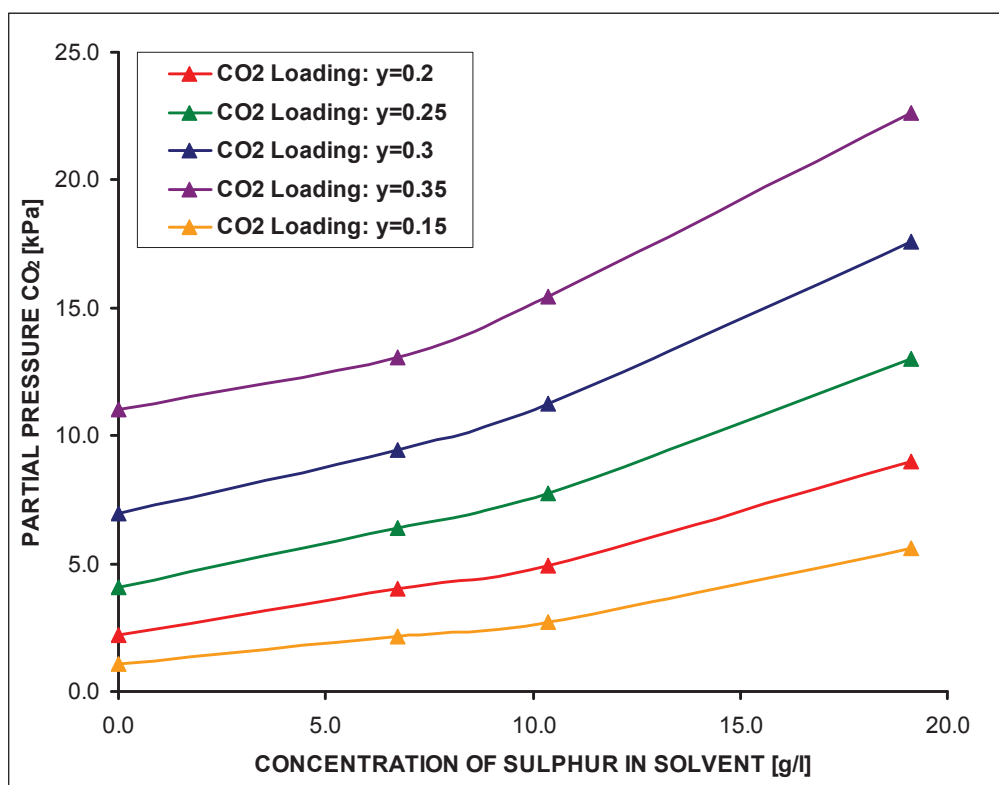


Figure 34: Effect of solvent sulphur concentration on the CO<sub>2</sub> equilibrium partial pressure at 100°C.

## 4.5 Properties, Effects and Solutions for the Absorbed SO<sub>2</sub>

Both the solubility and volatility provide relevant information of how the SO<sub>2</sub> can be treated following absorption. If the absorption reaction of sulphur dioxide is non - reversible at typical stripping conditions, it would imply that an accumulation of sulphur in the solution and consequently a decrease in the efficiency of CO<sub>2</sub> absorption will be observed. If however, the dissolved sulphur can be stripped from the solution, additional treatment following the stripper of the CO<sub>2</sub> – SO<sub>2</sub> stream will be necessary prior to compression of the CO<sub>2</sub> stream.

### 4.5.1 Volatility of Absorbed SO<sub>2</sub>

As mentioned earlier, it was not possible during the equilibrium experiment to determine whether the absorbed sulphur was re-released into the gas phase, due to the limitations of the GC column which was not able to detect SO<sub>2</sub>.

A series of other test were completed to determine whether Reaction(54) is reversible and hence SO<sub>2</sub> would be stripped from the solution. For this, a highly SO<sub>2</sub> loaded solution, prepared by a 1:1 dilution of SO<sub>2</sub> saturated solution, was heated to 100°C and the evolved gas stream was analysed using SO<sub>2</sub> specific Draeger–tubes. Draeger-tubes are glass vials filled with a chemical reagent that reacts with a specific gas. Using a Draeger pump, a

volume of the sample gas is drawn through the tube. If the analyte gas is present, the reagent in the tube changes colour and the length of the colour change gives a semi – quantitative measure of the gas concentration. The Draeger–tubes used in these experiments were for the detection of sulphur dioxide over a concentration range from 0.5 – 25ppm. It would be expected that the use of the high concentration SO<sub>2</sub> loaded solution, instead of a diluted solution, would result in a higher SO<sub>2</sub> concentration in the evolved gas phase and so enable better detection accuracy. That is, if the SO<sub>2</sub> could not be detected for the high concentration solution, it would not be detected for the lower concentration solution systems.

For the volatility tests, the equilibrium rig was set up as described in Section 3.1, however only one vessel was used. Several different measurement methods were attempted. Direct measurements of the gas stream with the Draeger-tube was found to be inaccurate, as the gas flow rate was too low in comparison to the volume required for the analysis. Another method was to collect the gas in a glass bottle and take samples of the collected gas after a couple of hours. The final and most accurate method was the collection of the gas in a gas tight plastic bag. After a couple of hours, samples of the collected gas were taken. With this method it was guaranteed that only the gas released from the equilibrium was analysed. The results of each of the different tests were negative, which would imply that no SO<sub>2</sub> was desorbed from the SO<sub>2</sub> loaded solution. The Draeger – tubes only tested for SO<sub>2</sub>, however, if other sulphur species were formed and desorbed from the solution into the gas phase they would not have been detected.

It would be concluded from these experiments that the absorption of SO<sub>2</sub> is a non – reversible reaction at the typical stripping operating conditions of 100°C and hence that the dissolved sulphur remains in solution. Consequently, sulphur species would accumulate in the solution during the flue gas absorption / stripping process, which inherently would have an effect on the CO<sub>2</sub> absorption performance. It is believed that possible solution to limit the sulphur concentration, would be the precipitation of sulphur.

#### 4.5.2 Solubility of Substances in Solution

The solubility of the different possible sulphur species in the K<sub>2</sub>CO<sub>3</sub> solution is important to investigate potential methods how the sulphur can be removed from the solution.

To determine the least soluble species in the SO<sub>2</sub>-CO<sub>2</sub>-K<sub>2</sub>CO<sub>3</sub> system, the K<sub>2</sub>CO<sub>3</sub> solution was loaded with SO<sub>2</sub> until precipitation was observed at room temperature. The solid formed was then analysed and observed to be potassium bicarbonate (KHCO<sub>3</sub>). A comparison with literature data [25], [27] would support the experimental results. Due to the fact that in the system no sulphate was present, as shown by the FTIR results presented in Section 4.3, it can be seen from Table 8 that bicarbonate is the least soluble of the species present in the system. These solubilities are valid for the species dissolved in water, a similar trend would be expected in the carbonate solution.



Table 8: Solubility of dissolved species in water.

	K <sub>2</sub> CO <sub>3</sub>	KHCO <sub>3</sub>	K <sub>2</sub> SO <sub>3</sub>	KHSO <sub>3</sub>	K <sub>2</sub> SO <sub>4</sub>
20°C	52.3	24.92	51.49	32.7	10
70°C	57.2	40.45	52.32	46.1	16.55

Solubilities expressed in mass percent of solute

Compared to the other compounds in Table 8, potassium sulphate is least soluble. At a temperature of 25°C the solubility of K<sub>2</sub>SO<sub>4</sub> is reported to be only 1.5w% in a 23.2w% potassium carbonate solution and only 0.3w% in a 35w% K<sub>2</sub>CO<sub>3</sub> solution [26]. No data is available in the literature for higher temperatures, but it can be assumed that the solubility would still be very low.

It could be concluded from this that it would be possible to precipitate the dissolved sulphur as potassium sulphate. Potassium sulphate can be formed by oxidising the potassium sulphite according Reaction(57). As a result of the lower solubility, the effect of the remaining dissolved sulphur on the equilibrium partial pressure of the CO<sub>2</sub> would be negligible low and the CO<sub>2</sub> absorption performance would not be affected adversely.

#### 4.5.3 Approximate Concentrations of Dissolved SO<sub>2</sub>

The following basic calculations give an approximately indication of the concentration of dissolved sulphur that could be expected in potassium carbonate solution based on practical values. For a typical CO<sub>2</sub> absorption packed column, the liquid – to – gas ratio (L<sub>M</sub>/G<sub>M</sub>) would be between 5 and 10. For an inlet flue gas SO<sub>2</sub> concentration of about 2000ppm and an outlet concentration of about 200ppm, which are typical values for coal fired power plants, the concentration of the dissolved sulphur in the potassium carbonate solution can be calculated as follows.

A sulphur mass balance over the absorption column is:

$$G_M \cdot (y_{SO_2 in} - y_{SO_2 out}) = L_M \cdot (x_{Sulphur out} - x_{Sulphur in}) \quad (72)$$

With the assumption that the inlet sulphur concentration of the solution is zero, the only unknown term is the outlet sulphur concentration of the solution after SO<sub>2</sub> absorption.

$$x_{Sulphur out} = 0.00018 - 0.00036 \frac{mol_{Sulphur}}{mol_{Solution}} \quad (73)$$

For a 30w% potassium carbonate solution with a concentration of 3.12 mol/l and a molecular weight of 32 g/mol for sulphur, the actual concentration of dissolved sulphur in the potassium carbonate solution is:



$$X_{\text{Sulphur out}} = 17.9 - 36 \frac{\text{mg}_{\text{Sulphur, solution}}}{I_{\text{K}_2\text{CO}_3 \text{ solution}}} \quad (74)$$

This implies that even after the absorption process of SO<sub>2</sub> and CO<sub>2</sub> into a fresh potassium carbonate solution the concentration of sulphur is relatively small, in comparison to the concentration of the absorbed CO<sub>2</sub>. For all experiments, discussed in Section 4.4, where a shift and with that a decrease of the CO<sub>2</sub> absorption performance was recorded, the concentration of sulphur was significantly higher. Despite a possible accumulation of sulphur in the solvent, the sulphur could be precipitated out as sulphate before any noticeable effect on the CO<sub>2</sub> absorption efficiency would occur.

## 5 Summary

Today, few dispute that the combustion of fossil fuels is one of the major causes of global warming and the greenhouse effect. By increasing the concentration of greenhouse effect contributing gases, in particular  $\text{CO}_2$ , more of infrared radiation and with that energy is absorbed and retained by the biosphere leading to an unavoidable increase in temperature of the lower atmosphere. It is reported that the earth has warmed by  $0.7^\circ\text{C}$  since 1900 [14] and with burning of more fossil fuels the warming will increase significantly. Even if increased energy efficiency, renewable energy sources and coal to gas substitution were to be widely implemented and utilised, it is unlikely that the ambitious goal of a stable  $\text{CO}_2$  concentration in the area of 500 – 600ppm could be achieved. Today, carbon capture and storage (CCS) is the believed by some to be the only feasible solution for a significant and immediate reduction in carbon dioxide emissions.

“CCS involves the use of technology, first to collect and concentrate the  $\text{CO}_2$ , transport it to a suitable storage location, and then store it away from the atmosphere for a long period of time. CCS would thus allow fossil fuels to be used with low emissions of greenhouse gases.” [13, pp. 19]

The three main approaches for capturing the  $\text{CO}_2$  generated from primary fossil fuels during power generation are post-combustion, pre-combustion and Oxyfuel combustion. Post-combustion is the only solution for the capture of  $\text{CO}_2$  from existing power plants without the need of enormous modifications. Many different solvents and solutions for the absorption of  $\text{CO}_2$  have been tested over the last few decades, most being either amine or carbonate based. The capture of  $\text{CO}_2$  with monoethanolamine (MEA) is only feasible from flue gases with low  $\text{SO}_2$  concentrations because the  $\text{SO}_2$  reacts with MEA leading to excessive solvent degradation. As an inorganic salt, potassium carbonate is resistant to irreversible chemical degradation by  $\text{SO}_2$  and has the ability to be used for the capture of  $\text{SO}_2$ . Various nitrogen oxide compounds ( $\text{NO}_x$ ) are another significant pollutant present in flue gases. It is believed that the capture of these compounds could also be possible using potassium carbonate based solutions.

To reduce the capital and operating costs of post-combustion flue gas treatment significantly, it is thought possible instead of using a multi-stage process flue gas treatment, with different units for the removal of  $\text{SO}_2$ ,  $\text{NO}_x$  and  $\text{CO}_2$ , that the  $\text{SO}_2$ ,  $\text{NO}_x$  and  $\text{CO}_2$  are simultaneously absorbed in one process unit. To achieve this, a solvent or solution that readily absorbs each needs to be utilised. Potassium carbonate based solutions are believed to be appropriate for absorption of these components in such a simultaneous manner.

Based on the overall goal to ascertain the feasibility of the industrial application of a one step simultaneous absorption of  $\text{SO}_2$ ,  $\text{NO}_x$  and  $\text{CO}_2$ , the individual aims of this work were determined. The main aim of this work was to investigate the effect of  $\text{SO}_2$  on the  $\text{CO}_2$  equilibrium curve and absorption efficiency of carbon dioxide using 30w% unpromoted potassium carbonate solution. As a consequence of the absorption of  $\text{SO}_2$  by the potassium



carbonate solution, the CO<sub>2</sub>-K<sub>2</sub>CO<sub>3</sub> system vapour-liquid equilibrium (VLE) curve will change. Depending on the observed change the absorption of SO<sub>2</sub> can have an effect on both the absorption performance and efficiency of the CO<sub>2</sub> capture unit. It is essential to know how the CO<sub>2</sub> equilibrium curve is altered by the absorption of SO<sub>2</sub> and how this will impact performance and efficiency. A quantitative relationship between the absorbed SO<sub>2</sub> and the resulting change in the equilibrium CO<sub>2</sub> partial pressure is a direct measure of this impact.

The identification of the SO<sub>2</sub> absorption reaction species and hence underlying reactions was another aspect of this work. These formed sulphur species were quantitatively analysed. Furthermore, investigation of the volatility and the solubility of these sulphur species in the carbonate solution give an indication of possible mechanisms by which the absorbed SO<sub>2</sub> and resulting sulphur levels can be regulated and purged from the solution.

In this study all the vapour-liquid equilibrium measurements were accomplished using a custom vapour – liquid equilibrium rig. The samples of the potassium carbonate solution were analysed for the carbonate and bicarbonate species using standard acid - base titration techniques. Analysis of the gas sampled from the equilibrium rig was performed on a Gas Chromatograph. Two different analytical techniques were used to analyse the dissolved SO<sub>2</sub> and resulting species. The total amount of dissolved sulphur in the potassium carbonate solution was measured by ICP - AES (Inductively Coupled Plasma - Atomic Emission Spectrometer). For a qualitative and semi-quantitative analysis of the sulphur species formed in the potassium carbonate solution, FTIR (Fourier Transform Infrared Spectroscopy) was used.

To verify the operation and validity of the vapour – liquid equilibrium rig, measurements for a CO<sub>2</sub> loaded 30w% potassium carbonate solution were made and compared to that reported in literature and predicted by the ASPEN PLUS simulation package. The overall reaction for the chemical absorption of CO<sub>2</sub> in potassium carbonate solutions can be described using the following equation,

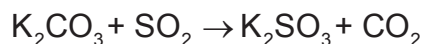


Due to the fact that the experimental results fit closely to that reported in the literature and the VLE simulations performed using ASPEN PLUS, it was concluded that the operating mode of the equilibrium rig was valid for the measurement of VLE at the desired operating conditions.

For study of the system SO<sub>2</sub> – CO<sub>2</sub> – K<sub>2</sub>CO<sub>3</sub> it was essential to first determine the sulphur species formed as a result of the absorption of SO<sub>2</sub>. The results of a qualitative and semi-quantitative FTIR analysis clearly imply that the absorbed SO<sub>2</sub> formed the sulphite species (SO<sub>3</sub><sup>2-</sup>). This was deduced from the fact that the measured sulphite concentration has an equivalent sulphur concentration to the total sulphur concentration as measured by ICP. This would also suggest that the main reaction that occurs during the absorption of SO<sub>2</sub> by the



potassium carbonate solution results in was the formation of sulphite and can be described by the following equation,



The formation of bisulphite ( $\text{HSO}_3^-$ ) as suggested in some literature was observed to be a minor side reaction as implied by the insignificant concentration of bisulphite measured. Other sulphur species like sulphate ( $\text{SO}_4^{2-}$ ) and bisulphate ( $\text{HSO}_4^-$ ) which could also be present as a result of subsequent side reactions were not observed in the analysis of the solution samples.

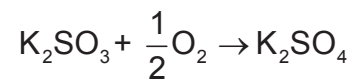
To investigate the effect of  $\text{SO}_2$  on the equilibrium partial pressure of  $\text{CO}_2$  over a 30w%  $\text{K}_2\text{CO}_3$  solution, experiments with three different total sulphur concentrations were made. It was evident from the experimental results that the absorption of sulphur dioxide by the potassium carbonate solutions resulted in a shift to the left of the  $\text{CO}_2$  vapour-liquid equilibrium curve. With increasing solution sulphur concentration, the curve was observed to shift further to the left with no alteration of the curve profile. This would imply that the form of the equilibrium curve is independent of the absorbed  $\text{SO}_2$  concentration. The main conclusion that can be drawn from these results is that the ability of the potassium carbonate solution to absorb  $\text{CO}_2$  from the gas stream decreases with increased levels of absorbed  $\text{SO}_2$ . Furthermore, during the absorption of  $\text{SO}_2$  and the subsequent formation of potassium sulphite, carbon dioxide is evolved and released. The released  $\text{CO}_2$  may then be directly re-absorbed by the carbonate solution to form bicarbonate. This would be equivalent to pre-loading of the carbonate solution with additional  $\text{CO}_2$ . As a direct consequence, the potassium carbonate solution would have a lower effective capacity to absorb  $\text{CO}_2$  from the flue gas stream. In effect, it results in a higher observed equilibrium partial pressure at a particular loading or conversely a lower loading for at a particular partial pressure.

Both the solubility and volatility of the various sulphur species that could form provide relevant information of how the  $\text{SO}_2$  could be treated following absorption by the potassium carbonate solution. To determine whether any  $\text{SO}_2$  could be stripped from a  $\text{SO}_2$  loaded carbonate solution, various tests were conducted using  $\text{SO}_2$  specific Draeger Tubes and highly  $\text{SO}_2$  loaded carbonate solutions. For each of these experiments no  $\text{SO}_2$  was detected by the Draeger Tubes, which would imply that no  $\text{SO}_2$  was desorbed from the solution. It was concluded from these experiments that the absorption of  $\text{SO}_2$  was non-reversible at the typical solution stripping temperature and pressure conditions of  $100^\circ\text{C}$  and  $101.3\text{kPa}$ . Hence, it would be expected that the dissolved sulphur remains in solution. As a consequence sulphur species would accumulate in the solution during the flue gas absorption / stripping process to a level that would inherently affect the  $\text{CO}_2$  absorption performance.

As mentioned earlier, the solubility of different possible sulphur species in the  $\text{K}_2\text{CO}_3$  solution is important to the investigation of potential methods by which the sulphur concentration in the potassium carbonate solution can be controlled. The least soluble species in the  $\text{SO}_2$ -



CO<sub>2</sub>-K<sub>2</sub>CO<sub>3</sub> system was reported in the literature and observed to be potassium sulphate (K<sub>2</sub>SO<sub>4</sub>). If oxygen or any other oxidant added to the solution, any sulphite can be partially reacted to form sulphate according to the following reaction equation,



As potassium sulphate has a very low solubility in the carbonate system, it is possible to precipitate out some of the dissolved sulphur. A reduction of the solution sulphur concentration by precipitation inherently reduces the adverse effect on the equilibrium partial pressure of the CO<sub>2</sub> and hence reduced CO<sub>2</sub> absorption performance that would otherwise be observed.

## 6 Indexes

### 6.1 References

- [1] Atkins, Peter; de Paula, Julio: Atkins' Physical Chemistry. 6<sup>th</sup> edition, New York: Oxford University Press Inc., 1998. - ISBN 0-19-879285-9
- [2] Perry, Robert H.; Green, Don W.; Maloney, James O.: Perry's Chemical Engineers' Handbook. 7<sup>th</sup> edition, New York: McGraw-Hill 1997. – ISBN 0-07-049841-5
- [3] Treybal, Robert E.: Mass – Transfer Operations. 3<sup>rd</sup> edition, Singapore: McGraw-Hill, 1981. – ISBN 0-07-066615-6
- [4] Kohl, Arthur; Nielsen, Richard: Gas Purification. 5<sup>th</sup> edition, Houston: Gulf Publishing Company, 1997. ISBN 0-88415-220-0
- [5] Coulson, J.M.; Richardson, J.F.: Chemical Engineering – Volume 2 Particle Technology & Separation Process. 4<sup>th</sup> edition, Oxford: Butterworth – Heinemann, 1997. – ISBN 0-7506-2942-8
- [6] Strigle, Ralph F. Jr.: Packed Tower Design and Applications – Random and Structured Packings. 2<sup>nd</sup> edition, Houston: Gulf Publishing Company, 1994. ISBN 0-88415-179-4
- [7] Schönbacher, Axel: Thermische Verfahrenstechnik – Grundlagen und Berechnungsmethoden für Ausrüstungen und Prozesse. Berlin: Springer, 2002. – ISBN 3-540-42005-3
- [8] Draxler, Josef: Skriptum zur Vorlesung Thermische Verfahrenstechnik. Leoben: Montanuniversität Leoben, Institut für Verfahrenstechnik des industriellen Umweltschutzes, 2002.
- [9] Nasir, Pervaiz; Mather Alan E.: The Measurement and Prediction of the Solubility of Acid Gases in Monoethanolamine Solutions at Low Partial Pressure. In: The Canadian Journal of Chemical Engineering, Vol. 55, December 1977.
- [10] Isaacs, Ezra E.; Otto, Fred D.; Mather Alan E.: Solubility of Mixtures of H<sub>2</sub>S and CO<sub>2</sub> in a Monoethanolamine Solution at Low Partial Pressures. In: Journal of Chemical Engineering Data, Vol. 25, 1980, S. 118 - 120



- [11] Astarita, Gianni; Savage, David W.; Bisio, Attilio: Gas Treating with Chemical Solvents. New York: John Wiley & Sons, Inc., 1983. - ISBN 0-471-05768-1
- [12] Tosh, J. S.; Field, J. H.; Benson H.E.; Haynes W.P.: Equilibrium Study of the System Potassium Carbonate Potassium Bicarbonate, Carbon Dioxide and Water. Report of Investigation, US Bureau of Mines, 1959.
- [13] Intergovernmental Panel on Climate Change: IPCC Special Report on Carbon Dioxide Capture and Storage. Cambridge: Cambridge University Press, 2005. - ISBN-13 978-0-521-86643-9 <http://www.ipcc.ch/pub/reports.htm>
- [14] Stern, Nicholas: Stern Review on the Economics of Climate Change: [http://www.hm-treasury.gov.uk/independent\\_reviews/stern\\_review\\_economics\\_climate\\_change/stern\\_review\\_index.cfm](http://www.hm-treasury.gov.uk/independent_reviews/stern_review_economics_climate_change/stern_review_index.cfm) (Stand: 27.November.2006)
- [15] Intergovernmental Panel on Climate Change: IPCC Third Assessment Report: Climate Change 2001. Cambridge: Cambridge University Press, 2001. <http://www.ipcc.ch/pub/reports.htm>
- [16] Intergovernmental Panel on Climate Change: IPCC Special Report Emissions Scenarios. Cambridge: Cambridge University Press, 2001. - ISBN: 92-9169-113-5 <http://www.ipcc.ch/pub/reports.htm>
- [17] Homepage von Cooperative Research Centre for Greenhouse Gas Technologies (CO2CRC): <http://www.co2crc.com.au/> (Stand: 28. November. 2006)
- [18] Hikita, H.; Asai S.; Takatsuka T.: Absorption of Carbon Dioxide into Aqueous Sodium Hydroxide and Sodium Carbonate – Bicarbonate Solutions. In: The Chemical Engineering Journal 11, Lausanne: Elsevier Sequoia S.A., 1976, S. 131 – 141
- [19] Savage, David W.; Astarita, Gianni; Joshi, Shriram: Chemical Absorption and Desorption of Carbon Dioxide from Hot Carbonate Solutions. In: Chemical Engineering Science Vol. 35, Pergamon Press Ltd, 1980, S. 1513 – 1522
- [20] Skoog, Douglas A.; West, Donald M.; Holler F.James: Fundamentals of Analytical Chemistry. 7<sup>th</sup> edition, Orlando: Saunders College Publishing, 1996. ISBN 0-03-005938-0
- [21] Beck, Brendan; Cook, Peter: Modelling the Potential of Geosequestration. In: Australasian Emissions Trading Forum, February/March 2005. [www.aetf.net.au](http://www.aetf.net.au)



- [22] Intergovernmental Panel on Climate Change: Climate Change 1992: The Supplementary Report to the IPCC Scientific Assessment. Cambridge: Cambridge University Press, 1992.
- [23] Stevens, Goeff: PowerPoint Presentation: CO<sub>2</sub> Capture and Separation Technologies (8.August 2004): <http://www.co2crc.com.au/understandccs.html> (Stand: 28.11.12006)
- [24] Kellner, R.; Mermet, J.-M.; Otto, M.; Widmer M.: Analytical Chemistry. Weinheim: Wiley – VCH Verlag, 1998. ISBN 3-527-28610-1
- [25] Stephan, M.; Stephan T.: Solubility of inorganic and organic compounds - Binary Systems – Part 1 and 2. Volume 1, Oxford: Pergamo Press LTD, 1963.
- [26] Seidell, Atherton: Solubility of inorganic and metal compounds. Volume 1, New York: D. Van Nostrand Company, 1953.
- [27] Platt, J.H.; Hudson, D.: The Solubility of Potassium Bisulphite. In: Journal – Society of Dyers and Colourists, Vol. 42, 1926, S. 348 – 349.
- [28] Bassett, J.; Denney, R.C.; Jeffery, G.H.; Mendham, J.: Vogel's Textbook of Quantitative inorganic Analysis. 4<sup>th</sup> edition, London – New York: Longman Group Limited, 1978. ISBN 0-582-46321-1
- [29] Hikita, H.; Asai S.: Gas Absorption with a Two – Step Chemical Reaction. In: The Chemical Engineering Journal 11, Lausanne: Elsevier Sequoia S.A., 1976, S. 123 – 129
- [30] Günzler, Helmut; Gremlich, Hans – Ulrich: IR Spectroscopy – An Introduction. Weinheim: Wiley – VCH Verlag, 2002. ISBN 3-527-28896-1
- [31] Potassium sulphite spectrum: <http://www.ijvs.com/spectra/k2so3.pdf> (Stand: 22. September 2006)
- [32] Homepage von FDM Reference Spectra Databases: <http://www.fdmspectra.com/> (Stand: 22.September 2006)
- [33] Pfennig, Andreas: Thermodynamik der Gemische. Berlin: Springer, 2004. ISBN 3-540-02776-9
- [34] Hikita, H.; Asai S.; Takatsuka T.: Gas Absorption with a Two – Step Instantaneous Chemical Reaction. . In: The Chemical Engineering Journal, Lausanne: Elsevier Sequoia S.A., 1971



- [35] Homepage von Dräger:  
[http://www.draeger.com/ST/internet/US/en/Products/Detection/Drager-Tubes/draeger\\_tubes.jsp](http://www.draeger.com/ST/internet/US/en/Products/Detection/Drager-Tubes/draeger_tubes.jsp) (Stand: 22. November 2006)
- [36] Gary, T.; Rochelle; Judson King, C.: The Effect of Additives on Mass Transfer in CaCO<sub>3</sub> or CaO Slurry Scrubbing of SO<sub>2</sub> from Waste Gas. In: Industrial Engineering Chemical Fundamentals Vol. 16, No. 1, 1977, S. 67 - 75
- [37] Recelj, T.; Golob, J.: Equilibrium and Mass Transfer in the Ca<sup>2+</sup> - SO<sub>2</sub> – H<sub>2</sub>O System of the Analysis of the Flue Gas Desulphurization Process. In: Trans IChemE, Part B, Process Safety and Environmental Protection, 2004, 82 (B5), S. 371 - 380
- [38] Walas, Stanley M.: Chemical Process Equipment. Newton: Butterworth – Heinemann, 1990. – ISBN 0-7506-9385-1
- [39] Bittrich, H.- J.: Leitfaden der chemischen Thermodynamik. Berlin: VEB Deutscher Verlag, 1971.
- [40] Wong, Sam; Bioletti, Rob: Carbon Dioxide Separation Technologie. Edmonton: Carbon & Energy Management Alberta Research Council, 2002.
- [41] Desideri, Umberto; Paolucci, Alberto: Performance modelling of a carbon dioxide removal system for power plants. In: Energy Conversion & Management 40. Elsevier Science Ltd., 1999, S. 1899 - 1915

## 6.2 Tables

Table 1: Range of total costs for CO <sub>2</sub> capture, transport and geological storage. ....	11
Table 2: Equilibrium constants for the absorption of CO <sub>2</sub> in K <sub>2</sub> CO <sub>3</sub> . ....	25
Table 3: Experimental equilibrium data points of CO <sub>2</sub> over 30w% potassium carbonate solution at 90 and 100°C. ....	52
Table 4: Total sulphur concentration of the loaded K <sub>2</sub> CO <sub>3</sub> solutions. ....	53
Table 5: Sulphite (SO <sub>3</sub> <sup>2-</sup> ) concentration of the loaded K <sub>2</sub> CO <sub>3</sub> solutions. ....	55
Table 6: Experimental results of the SO <sub>2</sub> and CO <sub>2</sub> equilibrium curve at 90°C. ....	58
Table 7: Experimental results of the SO <sub>2</sub> and CO <sub>2</sub> equilibrium curve at 100°C. ....	59
Table 8: Solubility of dissolved species in water. ....	64



## 6.3 Graphics

Figure 1: The greenhouse effect [14].	4
Figure 2: Atmospheric CO <sub>2</sub> concentration from 1850 – 2000 [14].	5
Figure 3: Past and future CO <sub>2</sub> atmospheric concentrations [15].	5
Figure 4: Variations of the Earth's surface temperature from 1765 to 2100.	6
Figure 5: Potential reduction of atmospheric CO <sub>2</sub> concentration with CCS.	8
Figure 6: Schematic diagram of possible CCS Systems [17].	8
Figure 7: Overview of CO <sub>2</sub> capture processes and systems [17].	9
Figure 8: Composition of total CCS costs.	10
Figure 9: Multi stage flue gas treatment including CO <sub>2</sub> capture.	12
Figure 10: Single-stage SO <sub>2</sub> , NO <sub>x</sub> and CO <sub>2</sub> capture process.	13
Figure 11: Raoult's Law, Henry's Law and real performance of a species i in solution [1].	17
Figure 12: Concentration profile for absorbed component A [5].	18
Figure 13: Driving Forces at the mass transfer.	20
Figure 14: Gas absorber using a solvent regenerated by stripping.	28
Figure 15: Design diagrams for absorption.	30
Figure 16: Design diagrams for stripping.	31
Figure 17: Effect of temperature and percentage conversion to bicarbonate on solubility of K <sub>2</sub> CO <sub>3</sub> plus KHCO <sub>3</sub> .	32
Figure 18: Flow diagram of hot potassium carbonate process with split stream.	33
Figure 19: Flow sheet of the double alkali flue gas desulphurization process.	34
Figure 20: Photo of the equilibrium rig.	36
Figure 21: Schematic of the equilibrium rig.	37
Figure 22: Typical titration curve for a loaded K <sub>2</sub> CO <sub>3</sub> solution.	41
Figure 23: Typical Gas Chromatogram with peaks for N <sub>2</sub> and CO <sub>2</sub> binary gas mixtures identified.	42
Figure 24: Calibration Curve for CO <sub>2</sub> and N <sub>2</sub> at GC settings of 240/120°C and 100mA.	43
Figure 25: Equilibrium curve of CO <sub>2</sub> over 30w% potassium carbonate solution at a water vapour pressure of 25°C.	50
Figure 26: Equilibrium curve of CO <sub>2</sub> over 30w% potassium carbonate solution at 90°C.	51
Figure 27: Equilibrium curve of CO <sub>2</sub> over 30w% potassium carbonate solution at 100°C.	51
Figure 28: FTIR spectrum of a CO <sub>2</sub> and SO <sub>2</sub> loaded solution.	54



Figure 29: Equilibrium curve of CO <sub>2</sub> over 30w% potassium carbonate solution at 90°C for different sulphur concentrations.....	57
Figure 30: Equilibrium curve of CO <sub>2</sub> over 30w% potassium carbonate solution at 100°C for different sulphur concentrations.....	57
Figure 31: Shifted equilibrium curves of the different sulphur concentrations at 90°C.....	60
Figure 32: Shifted equilibrium curves of the different sulphur concentrations at 100°C.....	60
Figure 33: Effect of solvent sulphur concentration on the CO <sub>2</sub> equilibrium partial pressure at 90°C.....	61
Figure 34: Effect of solvent sulphur concentration on the CO <sub>2</sub> equilibrium partial pressure at 100°C.....	62

